COLLEGE OF ENGINEERING

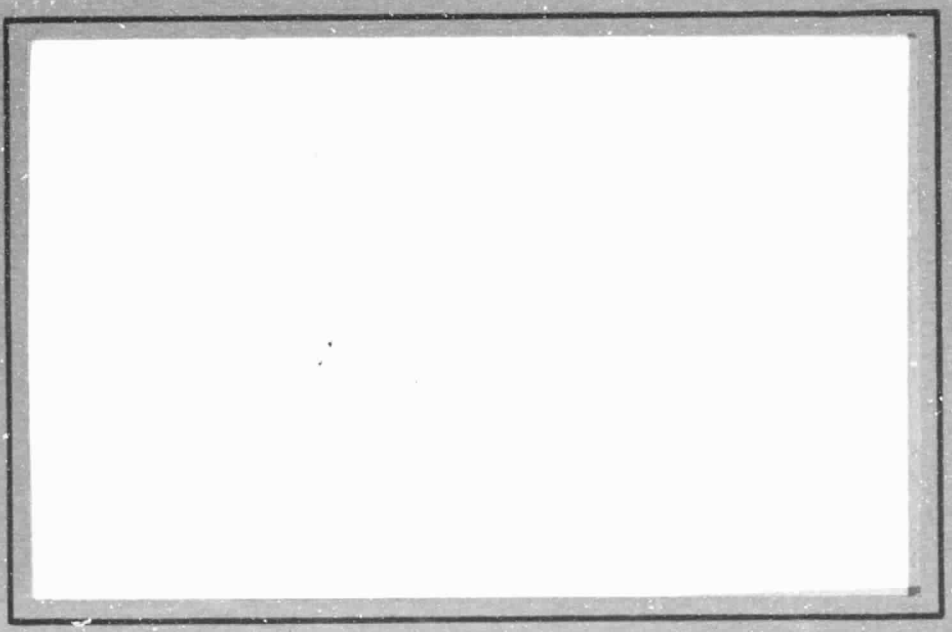

VIRGINIA POLYTECHNIC INSTITUTE AND STATE UNIVERSITY

BLACKSBURG, VIRGINIA

Investigation and Characterization of Constraint Effects on Flaw Growth During Fatigue Loading of Composite Materials

Final Report
NASA Grant NSG-1364

W. W. Stinchcomb, K. L. Reifsnider
P. Yeung, M. N. Gibbins

Engineering Science and Mechanics Department

Submitted to:

NASA Langley Research Center
Hampton, Virginia 23665

Materials Division
John Whitcomb, Monitor

June 1979

TABLE OF CONTENTS

OBJECTIVES OF THE INVESTIGATION

The nonideal behavior of composite materials, consisting of damage initiation, growth, and failure, has not, as yet, been adequately described due to an incomplete understanding of the mechanics of damage processes in these materials. A number of failure theories have been proposed which attempt to describe fracture of notched composites under quasi-static loads; however, efforts to extend these theories to the case of cyclic loading have achieved only partial success, at best, because the damage modes for static and cyclic loading are quite different.

There is a fairly large body of work covering a wide range of investigations on the fatigue behavior of composite materials [1]. The results of these investigations show that the state of damage in a composite material is strongly dependent on the material system, laminate configuration, geometry, stress state, loading history, and environment. From an applications viewpoint, one of the most important but incompletely answered questions concerns the fatigue response of notched composite materials.

One of the important factors controlling the fatigue damage processes in composites is the constraint imposed on a damaged (cracked) ply by adjacent (undamaged) plies. The initiation and growth of fatigue damage from a notch depends on the orientation of the major strength and stiffness directions in neighboring plies relative to the local stress state. At the present time, there is a lack of knowledge of the precise details of damage development around a notch in laminates and a corresponding lack of understanding of the influence of one lamina on the response of another lamina when they are bonded together as part of a laminate.

This report presents the results of an investigative program undertaken to attempt to add to the current understanding of constraint effects on the response of composite materials under cyclic loading. The objectives of this program were:

a) to use existing data and to develop additional data in order to establish an understanding and quantitative description of flaw growth in unidirectional lamina under cyclic loading at different load direction to fiber direction angles.

b) to establish a similar understanding and description of flaw growth in lamina which are embedded in laminates between other unflawed lamina.

c) to determine the nature of the influence of constraint on flaw growth by quantitatively comparing the results of the tests.

d) to develop a model and philosophy of constraint effects based on our investigative results.

APPROACH

The approach to attaining the objectives of the program was largely experimental. Analytical treatments of some of the behavior observed in the laboratory were carried out to assist in developing an understanding of the mechanics which applied to the response of the composites. The general approach was to attempt to completely and precisely determine the influence of constraint on the initiation, growth, and interaction of damage modes in composite laminates during several load histories. Secondly, the effect of the damage state on strength, stiffness, and lifetime was studied.

Static tension tests and tension-tension fatigue tests were conducted on sixteen types of T300/5208 graphite epoxy specimens as shown in Table I. The specimens were fabricated by Southwest Research Institute using pre-preg tape purchased from Narmco. Specimen types 1 and 2 are 1.0 inch wide by 7.0 inches long. Types 3 through 10 and type 15 are 1.5 inches wide by 7.0 inches long. Types 11 through 14 and type 16 are 1.5 inches wide by 10.0 inches long. The through the thickness notches are 0.250 inches long by 0.016 inches wide with a 0.008 inch radius at the notch tips. The notches were machined in the specimens using a 0.016 inch high speed diamond end mill. The embedded notches are through the center two plies of type 9, 10, 12, 14, 15 and 16 specimens. The notches in type 9, $[0,90]_s$ and type 12, $[\pm45,90]_s$, specimens are parallel to the fiber direction in the 90° plies. Type 10, $[90,0]_s$ and type 14, $[\pm45,0]_s$, specimens have notches which are perpendicular to the fiber direction in the 0° plies. The notches in type 15, $[90,0]_s$, and type 16, $[\pm45,0]_s$, specimens are parallel to the fiber direction in the 0° plies. These

TABLE I

GRAPHITE EPOXY TEST SPECIMENS

Type	Orientation	Number of Specimens Static	Number of Specimens Fatigue	Fiber Volume Fraction, %	Notch
1	$[0]_3$	3	5	52	Unnotched
2	$[90]_3$	3	5	52	Unnotched
3	$[0,90]_s$	3	5	64.9	Unnotched
4	$[90,0]_s$	3	5	66.5	Unnotched
5	$[0]_6$	3	5	66.6	Through slit parallel to fibers
6	$[0]_6$	3	5	65.6	Through slit perpendicular to fibers
7	$[90]_6$	3	5	64.7	Through slit parallel to fibers
8	$[90]_6$	3	5	64.2	Through slit perpendicular to fibers
9	$[0,90]_s$	3	5	63.6	Embedded slit in 90° plies parallel to fibers
10	$[90,0]_s$	3	5	61.7	Embedded slit in 0° plies perpendicular to fibers
11	$[\pm45,90]_s$	3	5	65.0	Unnotched
12	$[\pm45,90]_s$	3	5		Embedded slit in 90° plies parallel to fibers
13	$[\pm45,0]_s$	3	5	63.8	Unnotched
14	$[\pm45,0]_s$	3	5	63.8	Embedded slit in 0° plies perpendicular to fibers
15	$[90,0]_s$	3	5	65.6	Embedded slit in 0° plies parallel to fibers
16	$[\pm45,0]_s$	3	5	64.9	Embedded slit in 0° plies parallel to fibers

notches were made by milling the notch in the two pre-preg plies simultaneously, filling the void with liquid silicone rubber (RTV-21) and curing. The silicone rubber has no tensile or shear strength before or after cure.

Mechanical Tests

All tests were run using a 20 Kip MTS testing machine operated in the load control mode. Load ranges were selected for maximum accuracy and reproducibility.

Static Tests

Three specimens of each type were subjected to static tension tests to determine the mean values of tensile strength, elastic modulus, and fracture strain shown in Table II. Strain data were obtained from strain gages and an extensometer attached to the specimens. Stacked strain rosettes were also attached to the through-the-thickness notched specimens at the notch tips to measure any localized response. Similar gages were mounted on the outside surfaces of specimens with embedded flaws above the tips of the interior flaws. The time resolved local behavior of the material in the neighborhood of the notch tips was recorded on video tape during the tests. Visual observations of response were made by re-playing the tape and noting the changes in the damage state during the test.

Fatigue Tests

The tension-tension fatigue tests were run at a stress ratio of R = 0.1 and a frequency of 10 Hz. The maximum cyclic stresses were selected using the static tensile strength values as a data base. A slow rate

TABLE II

AVERAGE TENSILE PROPERTIES OF GRAPHITE EPOXY SPECIMENS

Specimen Type	Orientation	*Tensile Strength (KSI)	Elastic Modulus (MSI)	Fracture Strain (%)
1	$[0]_3$	141.7 ± 10.1	17.6 ± 0.7	0.77 ± 0.06
2	$[90]_3$ (first test)	4.83 ± 0.4	1.31 ± 0.03	0.37 ± 0.0
2	$[90]_3$ (second test)	5.49 ± 0.8	1.34 ± 0.01	0.50
3	$[0,90]_s$	86.3 ± 17.0	9.64 ± 0.72	0.81 ± 0.12
4	$[90,0]_s$	100.7 ± 14.1	10.14 ± 2.2	0.97 ± 0.30
5	$[0]_6$	154.6 ± 20.3		
6	$[0]_6$	72.8 ± 11.8		
7	$[90]_6$	3.44 ± 0.30		
8	$[90]_6$	6.27 ± 0.65		
9	$[0,90]_s$	105.3 ± 9.64		
10	$[90,0]_s$	82.0 ± 0.90		
11	$[\pm45,90]_s$	25.0	3.44	1.06
12	$[\pm45,90]_s$	25.6		
13	$[\pm45,0]_s$	85.6	7.96	1.16
14	$[\pm45,0]_s$	51.5		
15	$[90,0]_s$	113.1		
16	$[\pm45,0]_s$	76.6		

* Strength values calculated using net section areas for specimens with through the thickness notches.

loading ramp was applied to bring the specimen to the desired mean load, and the elastic modulus was determined. A sinusoidal loading function of the desired amplitude was then superimposed on the mean load to achieve a specific cyclic loading condition. The specimens were cycled at a constant maximum stress until fracture or 10^6 cycles, whichever occurred first. Typically, the test was interrupted at 1/2, 5×10^3, 1×10^4, 5×10^4, 1×10^5, 3×10^5 and 7×10^5 cycles to allow various nondestructive techniques to be applied to determine the damage development in the specimen.

Specific details of the mechanical tests and results are given in References 2 and 3.

Damage Detection

A number of investigative methods were employed before, during, and after the mechanical tests to measure the response of the material and determine the damage state in the specimens. The methods include:

- microscopy
- ultrasonic c-scan
- ultrasonic attenuation
- acoustic emission
- replication
- x-radiography
- stiffness
- thermography
- sectioning.

The analytical work used to assist in the interpretation of data and representation of the damage process includes:

- a laminated plate theory stress analysis with thermal residual stress and interlaminar normal stress approximation
- a one-dimensional model of a characteristic damage state in unnotched laminates
- a three-dimensional finite difference solution of the stress balance equations for the embedded flaw problems.

During the static and fatigue tests, attempts were made to follow the initiation and development of damage in a nondestructive manner. When possible, these investigations were carried out in real time or with only short interruptions in the loading history. Several newly developed nondestructive investigation methods and a number of more common methods have been used in concert to monitor damage development and assist in the interpretation of results. A brief description of each technique follows:

1. Microscopy - Light microscopy was used to observe the details of cracks and delaminations. Although a traveling light microscope can be attached to the testing machine to observe damage details during static tests, this form of microscopy is limited in that it provides a localized field of view and requires a long time to scan and photograph the entire specimen. In many cases, the damage events just prior to fracture occurred outside the field of view of the microscope. This form of light microscopy was replaced by the replication technique.
2. Ultrasonic c-scan - The c-scan is one of the more frequently used nondestructive methods for inspection of composite materials. It is particularly suited for detecting defects in the plane

of a laminate plate and mapping regions of relative good and bad quality in the plate. However, it is not possible to quantify the severity of a defective region on an absolute scale and the data is most accurately interpreted when it is compared to a c-scan of a calibrated test standard. In the present investigation, the c-scan was primarily used to determine the initial condition of the specimens and the extent of delamination around the embedded notches.

3. Ultrasonic attenuation - The ultrasonic pulse-echo method measures attenuation in thin composite laminates with the use of a buffer block for time resolution of the pulses. An analysis of the path followed by the echos in the specimen and buffer block indicates that the measured changes in ultrasonic attenuation can be accounted for by diffraction or scattering effects caused by the developing damage state in the material. The pulse-echo method is particularly sensitive to the initiation of damage in the interior of composite laminates and has been used on a number of different laminate configurations. It provides a very distinct indication of damage initiation which has been verified by other methods such as sectioning, x-radiography, and acoustic emission.

4. Acoustic emission - During several static tension tests, acoustic emission was monitored to detect the initiation of damage in the laminates. Although acoustic emission data is difficult to interpret in terms of discrete damage events (matrix cracks, fiber fracture, delamination, etc.), the data are consistent with observations made using other techniques.

5. Replication - In the replication method, cellulose acetate tape is softened with a diluted acetone solution and pressed against the surface where cracks are thought to exist. The tape flows into the surface detail and hardens. When the tape is removed, a record of the surface detail is obtained. The image on the tape can then be viewed in a microscope or reproduced on film for inspection. The replication process allows magnification of 50X to 100X without the depth of field limitations inherent to light microscopy so that the method is actually preferable to direct observation using a standard microscope. Replicas are made at different load levels and/or different numbers of loading cycles. Replicas are also made of surfaces created by sectioning specimens which have undergone fatigue loading and have developed some damage. These replicas are used to document the damage in the vicinity of an embedded flaw.

6. Radiography - The acceptance of x-radiography as a common nondestructive evaluation technique for graphite epoxy composites has been impeded by the need to use an image enhancement agent, such as tetra-bromoethane (TBE), to make the damaged regions opaque to x-rays. However, it is possible in some instances to create a situation which permits "soft" x-radiography of graphite epoxy without the need for an image enhancement agent. Although all aspects of the technique are not completely understood at the present time, some success has been achieved in our laboratory in resolving the details of internal damage such as matrix cracks.

7. Stiffness - Unlike strength, stiffness decreases monotonically with damage and the change in stiffness can be monitored to follow the development of damage throughout the loading history. In some design situations, stiffness changes may be incorporated in the failure criterion. Change in stiffness data correlates very well with data from other techniques which measure damage in composite laminates. Specifically, a sharp change in ultrasonic attenuation and, in some cases, acoustic emission count rate are coincident with a knee or step in the static stress strain curve. The change in stiffness during cyclic loading of laminates with embedded flaws is an indicator of damage development whereas residual strength is not.

8. Thermography - Video thermography is a real time thermal imaging method which can be used to detect damage initiation and follow damage growth in composite materials. The method is directly applicable to damage studies in composites since it is able to assess the combined effect of the multiple damage modes which form the damage state. Damage events dissipate energy as heat which can be detected by a thermographic camera. By distinguishing between steady state stress field related heat dissipation and transient heat development, it is possible to determine the severity of defects and monitor the propagation and distribution of flaws.

9. Sectioning - In order to completely and precisely determine the nature and extent of damage in the composite laminates, a large number of specimens with monotonic and cyclic loading

histories were sectioned and examined using the replication method. Sectioning studies aid in the interpretation of the nondestructive investigation data and provide a detailed description of the damage state along the length and through the width of the specimen. The results of these studies are presented in this report.

In order to accurately assess the effect of the different constraining plies on a given flaw situation, a common loading parameter is needed so that the local behavior of different laminates can be compared under at least one identical condition. As a first attempt at identifying an appropriate parameter, the nominal stress in the flawed ply was selected. Specifically, the total loads to be applied to type 10 ($[90/0]_s$ with an embedded flaw in the interior 0° plies) and type 14 ($[\pm45/0]_s$ with an embedded flaw in the interior 0° plies) specimens were calculated, using laminated plate theory, to produce the same nominal stress in the 0° plies in each laminate. For example, in order to produce nominal axial stress in the interior 0° plies of each laminate equal to 70 percent of the notched tensile strength of a unidirectional laminate (type 6 specimen), a $[90/0]_s$ laminate must be stressed to 36 percent of its ultimate tensile strenght (UTS) whereas a $[\pm45/0]_s$ laminate must be stressed to 41 percent of its tensile strength. These values were calculated using laminated plate theory to include the mechanical and thermal curing stresses. For specimens 1.5 inches wide, the axial stresses in the 0° plies are:

$$\sigma_{x0°} = 52.0\ P - 6.04 \text{ for } [90/0]_s \text{ laminates and}$$

$$\sigma_{x0°} = 41.9\ P + 1.44 \text{ for } [\pm45/0]_s \text{ laminates where}$$

the stresses are in ksi when the applied load, P, is in kips.

SECTIONING STUDIES

In order to determine the extent of the internal damage around the embedded flaw, and to relate with results as obtained by the nondestructive investigations, some specimens were sectioned and replicated.

Transverse sections were made on type 10 specimens (as shown schematically in Fig. 1) and on type 14 specimens. The sections were made by sawing the specimen just above the transverse axis of the flaw and polishing the cut surface to the flaw position. Subsequent sections were made by cutting and polishing at locations above and below the horizontal axis. Replicas of the polished surface were formed by pressirg a piece of 10 mil cellulose acetate tape, wetted with acetone, against the surface. The replica forms a permanent record of the damage detail on the entire surface of the section and can be studied in a microscope or used to make photographic prints.

Reproductions of a series of replicas made on a $[\pm 45,0]_s$ flawed laminate are shown in Fig. 2. The specimen had been fatigued at a stress level equal to 85 percent of the average tensile strength of the laminate for 200,000 cycles before being sectioned. The $X = 0$ replica shows the transverse section through the embedded flaw. The arrows indicate the flaw position with respect to the width of the specimen. The fatigue damage of the type 14 specimen consists of delamination of the +45/-45 and the -45/0 interfaces, axial cracks along the fiber direction in the ±45° plies near the damage area, and axial splits originating at the tip of the flaw and running along the fiber direction in the interior 0° plies. The length of the axial splits and the extent of the delaminations were measured on the replicas and original photomicrographs, and the

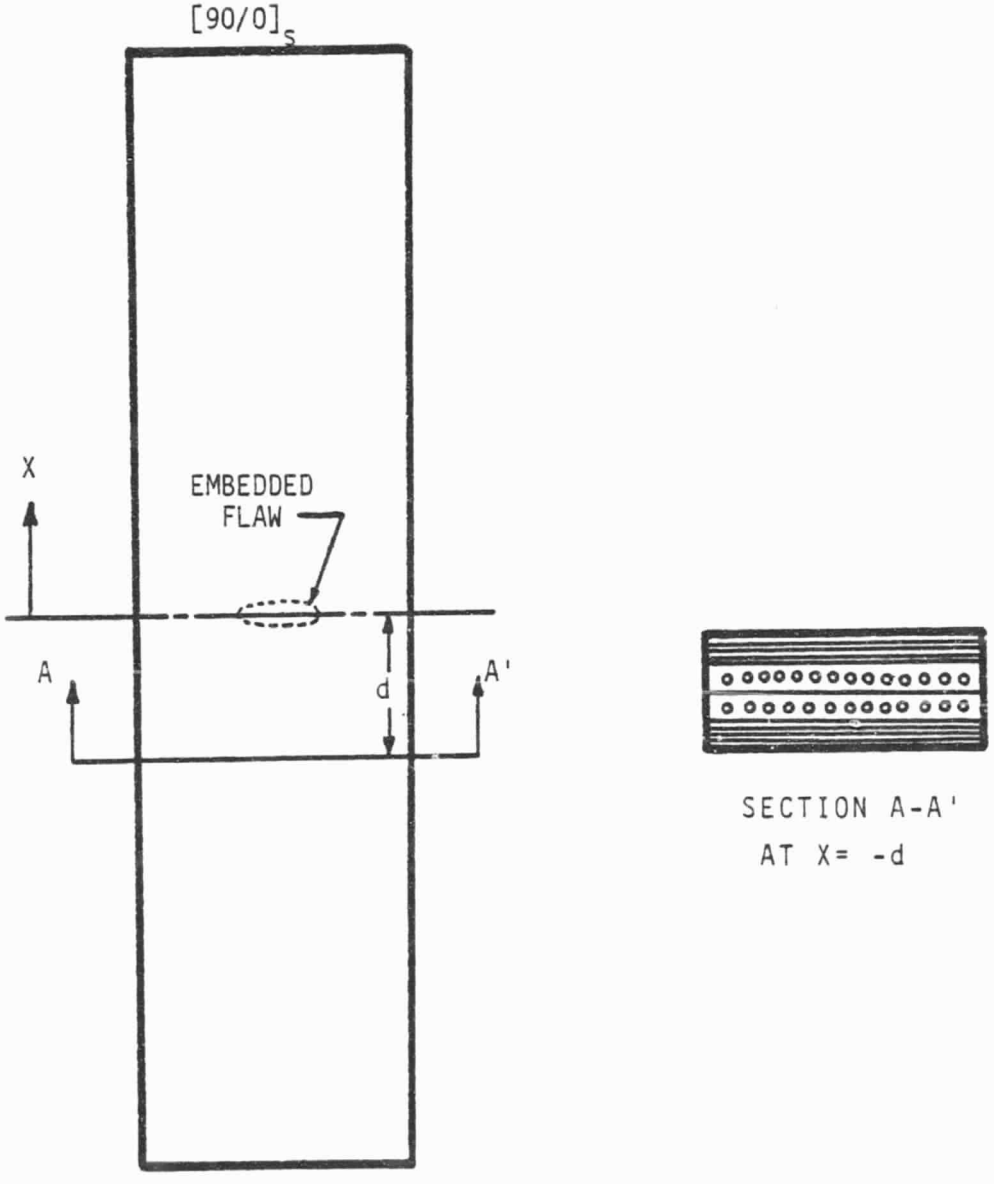

Fig. 1. Schematic diagram of sectioning studies on a typical $[90,0]_s$ type laminate with a flaw embedded transversely in the interior 0° plies.

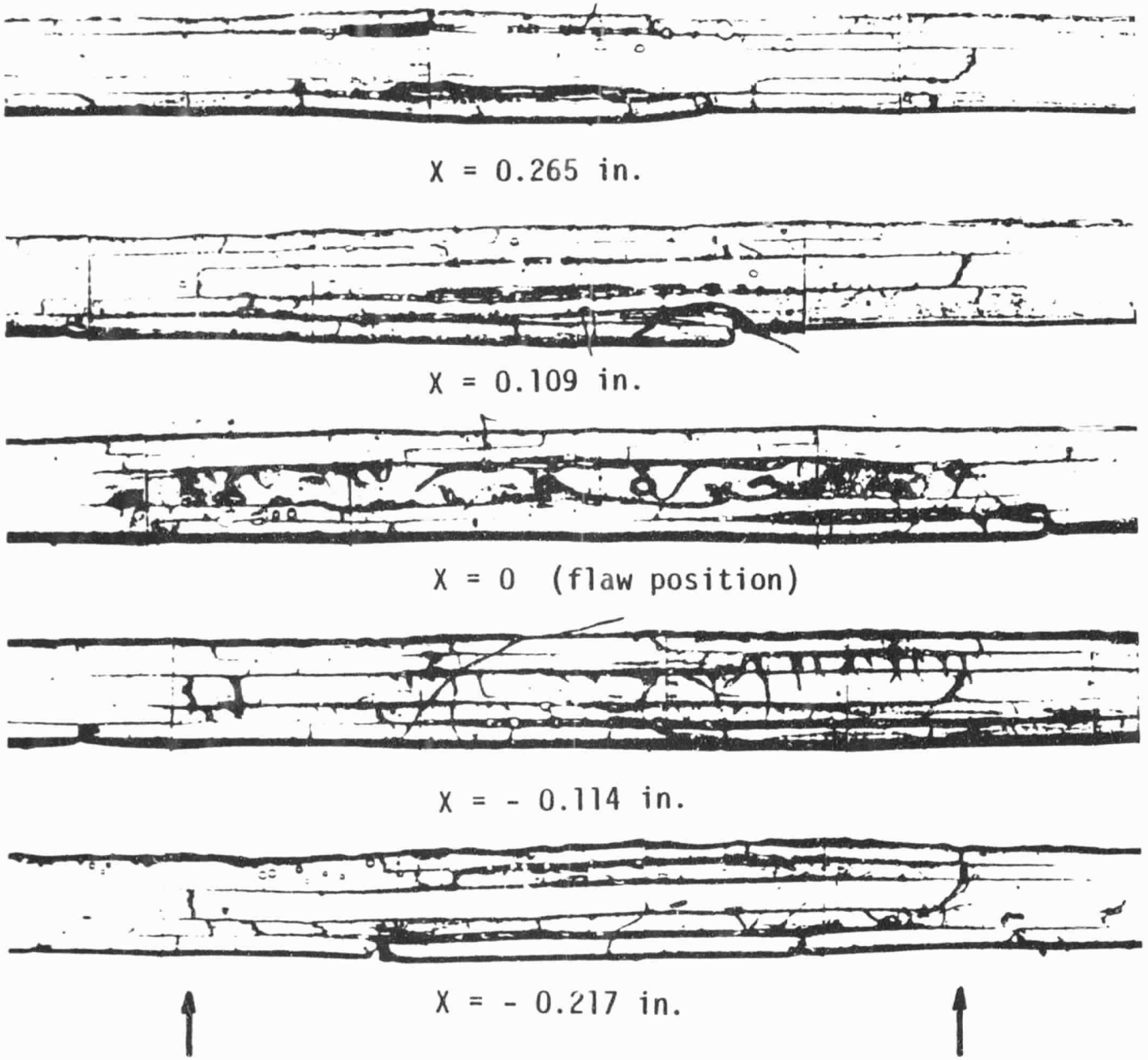

Fig. 2. Sectioning studies of a type 14 $[\pm 45,0]_s$ laminate with a notch embedded in the interior 0° plies, after 200,000 cycles of fatigue loading at 85% UTS. The nominal axial stress in the 0° plies is 134% of the notched tensile strength of the type 6 specimens.

results are presented in Fig. 3. The figures are constructed with the aid of a Tektronix 4051 computer and graphics system.

To assist in the interpretation of the data, the results are presented for (A), delamination of the upper +45/-45 interface and (B), delamination of the upper -45/0 interface and (C), delamination of the lower 0/-45 interface and (D), delamination of the lower -45/+45 interface and (E), a combined drawing showing the maximum extent of delamination in a 2-dimensional plane view and the length of the axial splits in the interior 0° plies. The transverse lines indicate the extent of delamination as measured from the replica made at that particular sectioning location. The vertical lines in Fig. 3E show the length of the axial splits in the interior 0° plies and suggest that these axial cracks are confined to the damaged region around the flaw and do not extend beyond the delaminated zone. The c-scan of the same specimen after 200,000 cycles is shown in Fig. 3F, and the shape and size of the delaminated region described by the sectioning data correlate well with the c-scan result.

There is also good agreement between the size and shape of the delaminated region in the c-scan and that obtained from sectioning studies for a type 10 $[90,0]_s$ flawed laminate. For this particular orientation of the constraining unflawed plies, however, the axial splits at the tips of the embedded flaw in the interior 0° plies tend to propagate beyond the delaminated region. Since the ultrasonic c-scan can only detect planar delamination perpendicular to the direction of travel of the sound wave, other nondestructive techniques (such as x-ray radiography) have to be used to determine the actual length of these interior axial splits.

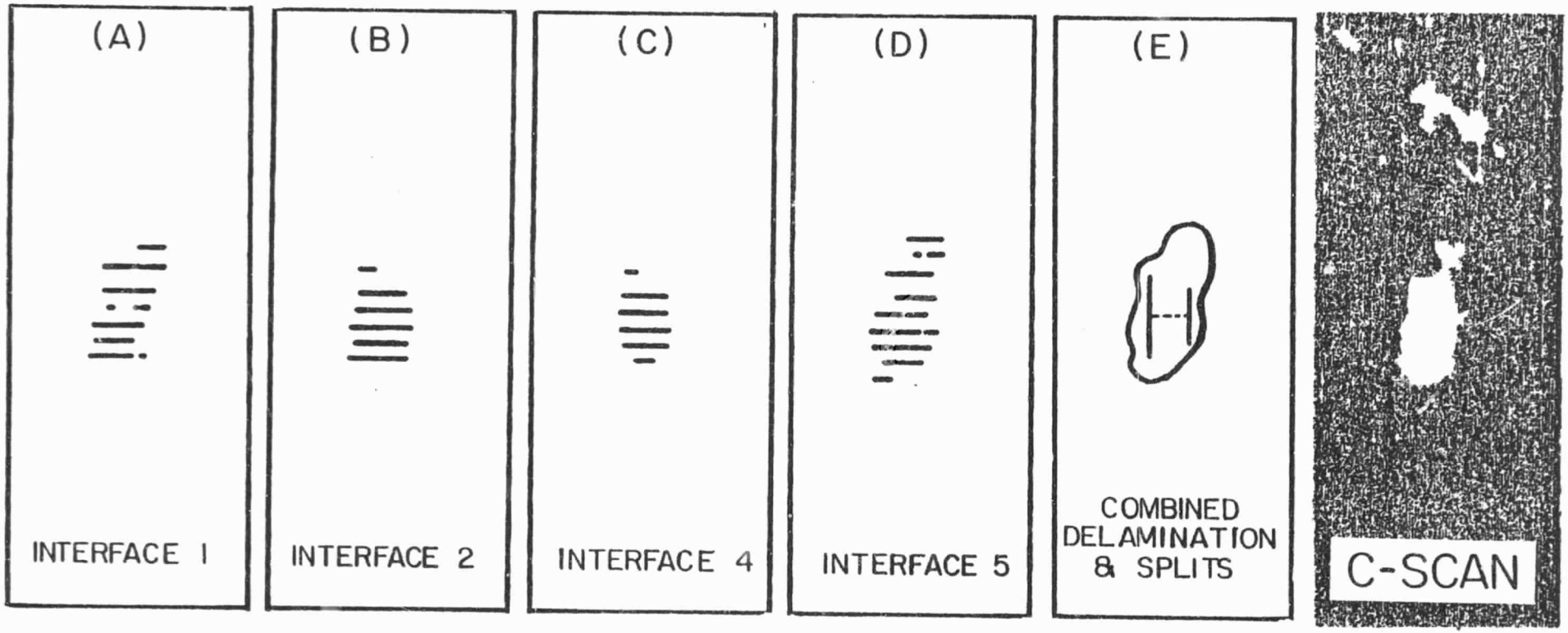

Fig. 3. Results of sectioning studies on a type 14 ($[\pm 45,0]_S$ with embedded flaw) specimen after 200,000 cycles of fatigue loading at 85% UTS. (A) +45/-45 interface; (B) -45/0 interface; (C) 0/-45 interface; (D) -45/+45 interface; (E) combined diagram of delamination and axial splits in the interior 0° plies; and (F) c-scan of the same specimen. Diagrams are approximately actual size.

RESULTS

The following section is a summary of results of the damage initiation and growth for the flawed laminates under monotonic and cyclic loading conditions. In all cases, the flaw is located in the interior 0° plies and is oriented either in the direction of the fibers or transverse to the fiber direction. Summaries of the response of the unflawed laminates and laminates where the flaw is located in 90° plies are given in earlier reports [2-4].

Static Tests

Axial cracks initiated at the notch tips of the transversely notched $[0]_6$ (type 6) specimens as matrix cracks at approximately 25 percent of the failure load. These cracks then extended along the fiber direction and propagated towards the ends of the specimens as the load was increased. The final failure was usually associated with the complete separation of the specimen into two parts along the longitudinal cracks which developed.

The response of a similarly notched lamina when constrained by unflawed laminae on both sides was quite different. In the case of a type 10 specimen where the constraining plies were 90° plies, transverse cracks in the exterior 90° plies were observed to develop at the notch location at stresses of approximately 20 ksi (138 MPa) and grow to a length slightly longer than the notch at 45 ksi (310 MPa). Between 40 ksi (276 MPa) and 70 ksi (483 MPa), surface creases in the 90° plies above and below the notch were observed where cracks developed at the notch tips in the interior 0° plies and extended parallel to the fibers.

Figure 4 shows the ultrasonic attenuation measured across the flawed region for a type 10 specimen while being quasi-statically loaded

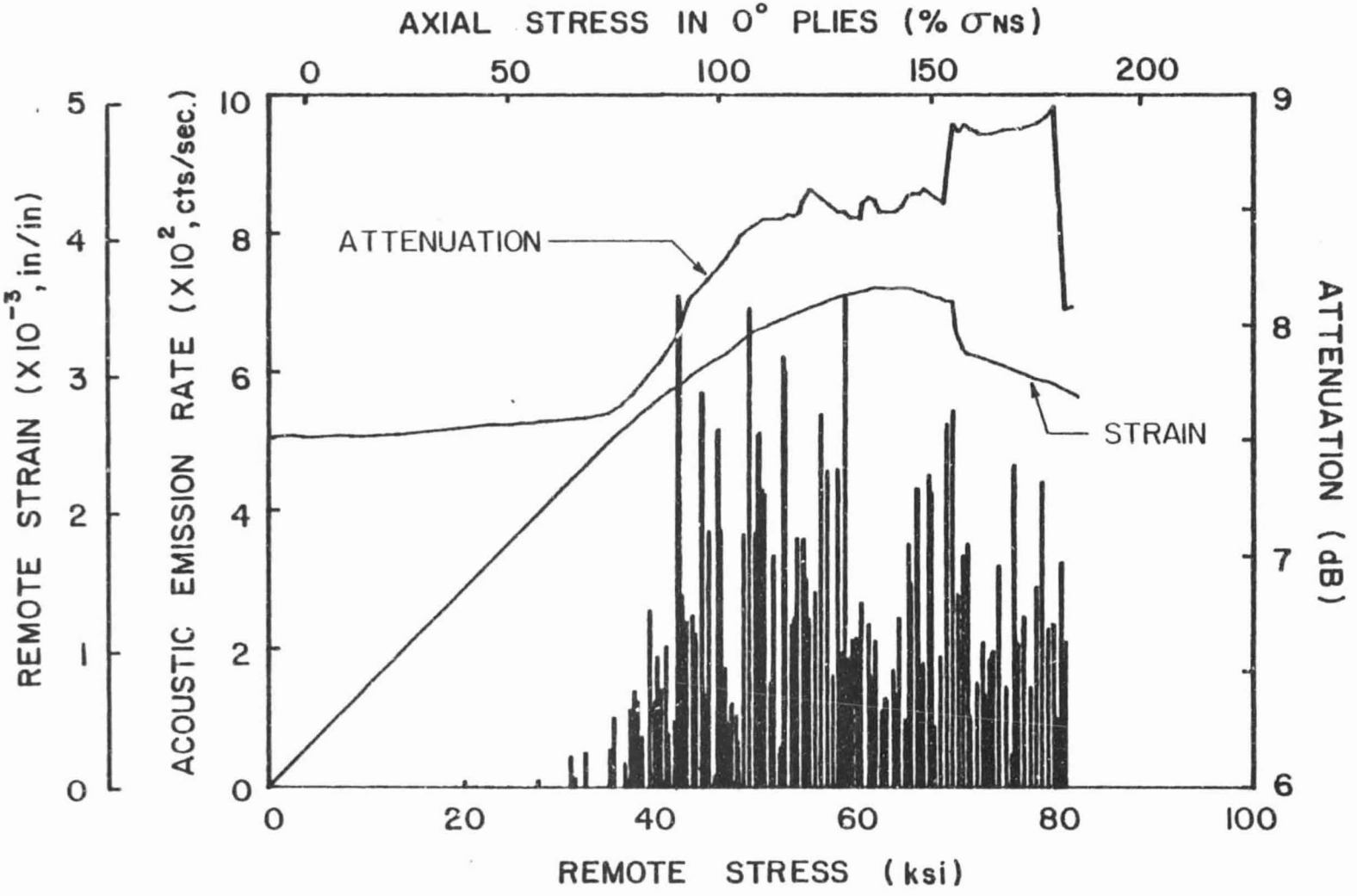

Fig. 4. Acoustic emission rate, attenuation, and remote strain vs. applied stress for a type 10 ($[90,0]_s$ with a transverse flaw in the interior 0° plies) specimen loaded statically to failure.

to failure. Superimposed on the same diagram are the acoustic emission (A.E.) rate and longitudinal strain variations during the loading sequence. The strain gage was mounted approximately one half inch below the flaw location. Significant acoustic emission was detected when the remote stress reached a value of approximately 37 ksi (255 MPa), and continued thereafter until fracture. At about the same stress level, the stress-strain behavior as measured by the remote strain gage began to deviate from linearity, and this was accompanied by a sudden change in the ultrasonic attenuation measurement across the flaw location. Since this is above the stress level at which the 90° plies began to separate at the flaw location, we can assume that the acoustic emissions detected are not entirely due to the cracking of the 90° plies. The sudden increase in attenuation measurement over the embedded flaw, however, suggests that axial cracks might be developing at the tips of the notch along the fiber direction in the interior 0° plies. The existance of these cracks relaxes the stress state of the region, causing a relaxation of strain measured by a remote gage mounted on the outer 90° plies in the region of the ligament. Hence, the presence of the constraining 90° plies provides additional transverse stiffness to the interior 0° plies, increasing the stress level at which these axial cracks develop when compared to the unconstrained case (type 6 specimens).

The stress level at which the A.E. rate begins to increase was repeatable over several tests and remained approximately the same for tests without the ultrasonic attenuation transducer where the restraint from the positioning and clamping of the transducer directly above the flaw is eliminated. The final failure mode of the type 10 specimens was

a transverse fracture of 0° plies initiating at the axial internal cracks.

When a biaxial state of constraint was imposed on transversely notched 0° plies, such as in the case of type 14 specimens, where the constraining plies were oriented at ±45°, the response of the laminate was significantly different. Figure 5 shows a typical plot of the variation of the measured parameters for a $[\pm 45,0]_s$ flawed laminate under monotonic loading. There were occasional bursts of A.E., but the pattern was not consistant. The stress-strain behavior was linear until just before fracture. The attenuation across the flawed region continuously increased for this specimen but no detectable damage was observed. Fractures of these specimens were through the embedded flaw with the failure of the 0° plies extending away from the notch tip at 45° to the fiber direction. The remaining portion of the specimen failed transverse to the loading direction. Splitting of internal 0° plies at the notch tip was detected in some cases, but did not act as a major part of the static fracture.

The importance of constraint effects on the behavior of the transversely notched 0° plies can be demonstrated by comparing the tensile strength data of the flawed specimens. The notched unidirectional 0° laminate failed at an axial net section stress of 72.8 ksi (502 MPa). Using laminated plate analysis, one can calculate the net section stress exerted on the 0° plies in the embedded flaw specimens. The net section stresses were 177 ksi (1220 MPa) in the case of 90° constraining plies (type 10 specimen) and 145.2 ksi (1001 MPa) in the case of ±45° constraining plies (type 14 specimen). It was obvious that some constraint effects

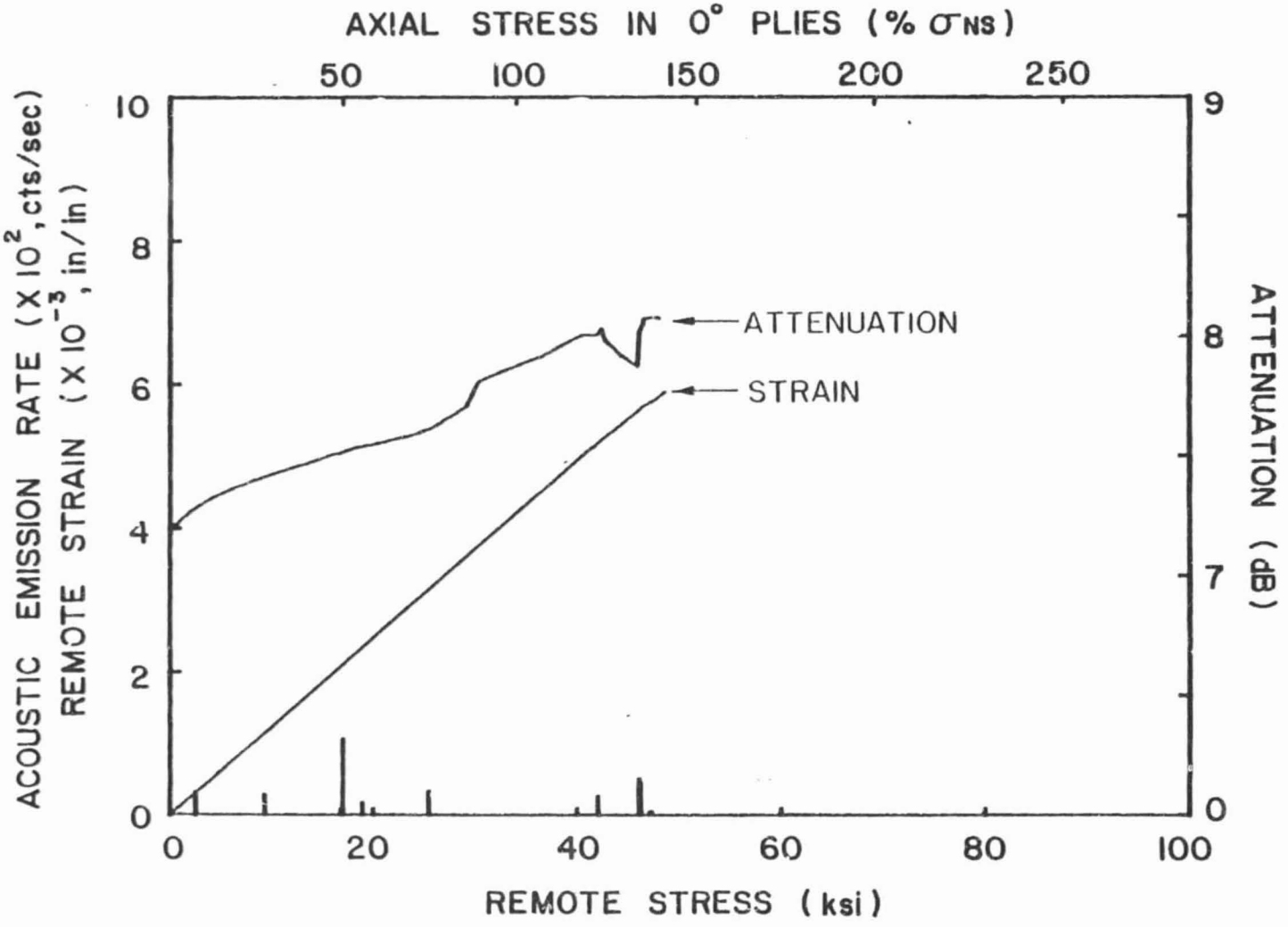

Fig. 5. Acoustic emission rate, attenuation, and remote strain vs. applied stress for a type 14 ($[\pm 45,0]_s$ with a transverse flaw in the interior 0° plies) specimen loaded statically to 2400 lbs.

were occurring since in both cases, the 0° ply stresses were higher than that of the unconstrained case. This is possibly due, in part, to the fact that any local stress concentration effect of the notch had been reduced by the presence of the constraining plies. More interpretation of this situation is offered in the final section of this report.

When the orientation of the notch in the 0° plies is parallel to the fiber direction, the A.E. and attenuation results exhibited similar trends for the orientation of the constraining plies. Figures 6 and 7 show the results for typical $[90,0]_s$, type 15, and $[\pm45,0]_s$, type 16, longitudinally flawed laminates respectively. Again, the A.E. events were more pronounced for the 90° constraining ply configuration. Although the major A.E. activity occurred at approximately 40 ksi (276 MPa), there was evidence of a subtle change in the attenuation across the flaw as early as 24 ksi (165 MPa), coupled with small A.E. events. There was considerably less acoustic emission for the $[\pm45,0]_s$ flawed specimens, and the attenuation remained stable until just before fracture. The failure modes for these specimens were not affected by the orientation of the constraining plies and in both cases, they were transverse to the loading axis and across the embedded flaw. However, there was some evidence of splitting in the interior 0° plies for the $[90,0]_s$ specimens away from the flaw.

The manner in which these interior 0° plies failed was quite different when compared to that of type 5 specimens. In the unconstrained case, severe axial splitting was present both at the notch tips and across the width of the specimen before final fracture. The 90° constraining plies also produced a higher stress in the interior 0° plies of 185 ksi (1276 MPa) at fracture when compared to a tensile strength of 155 ksi (1069 MPa)

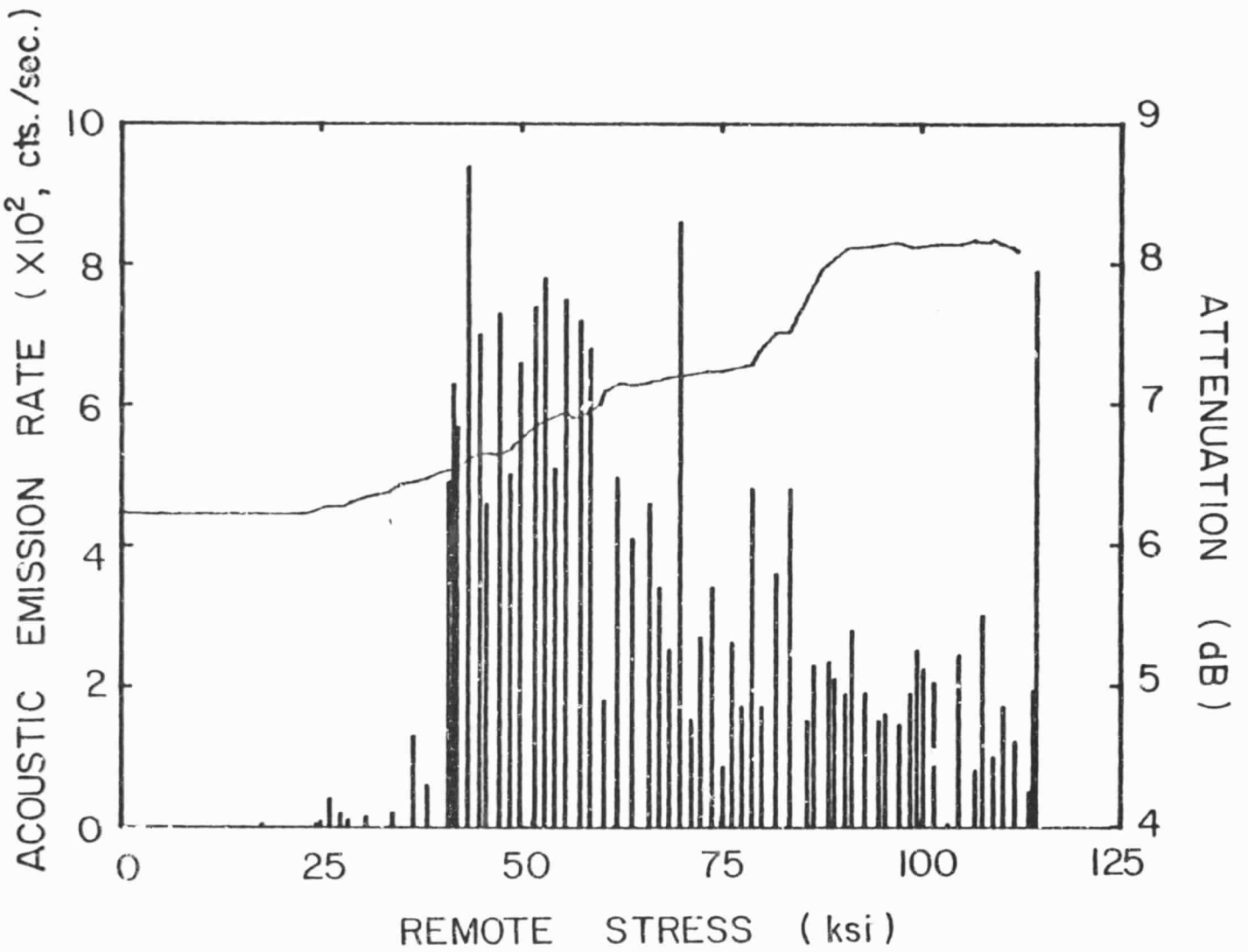

Fig. 6. Acoustic emission rate and attenuation vs. applies stress for a $[90,0]_s$ specimen with a longitudinal flaw in the interior 0° plies loaded statically to failure.

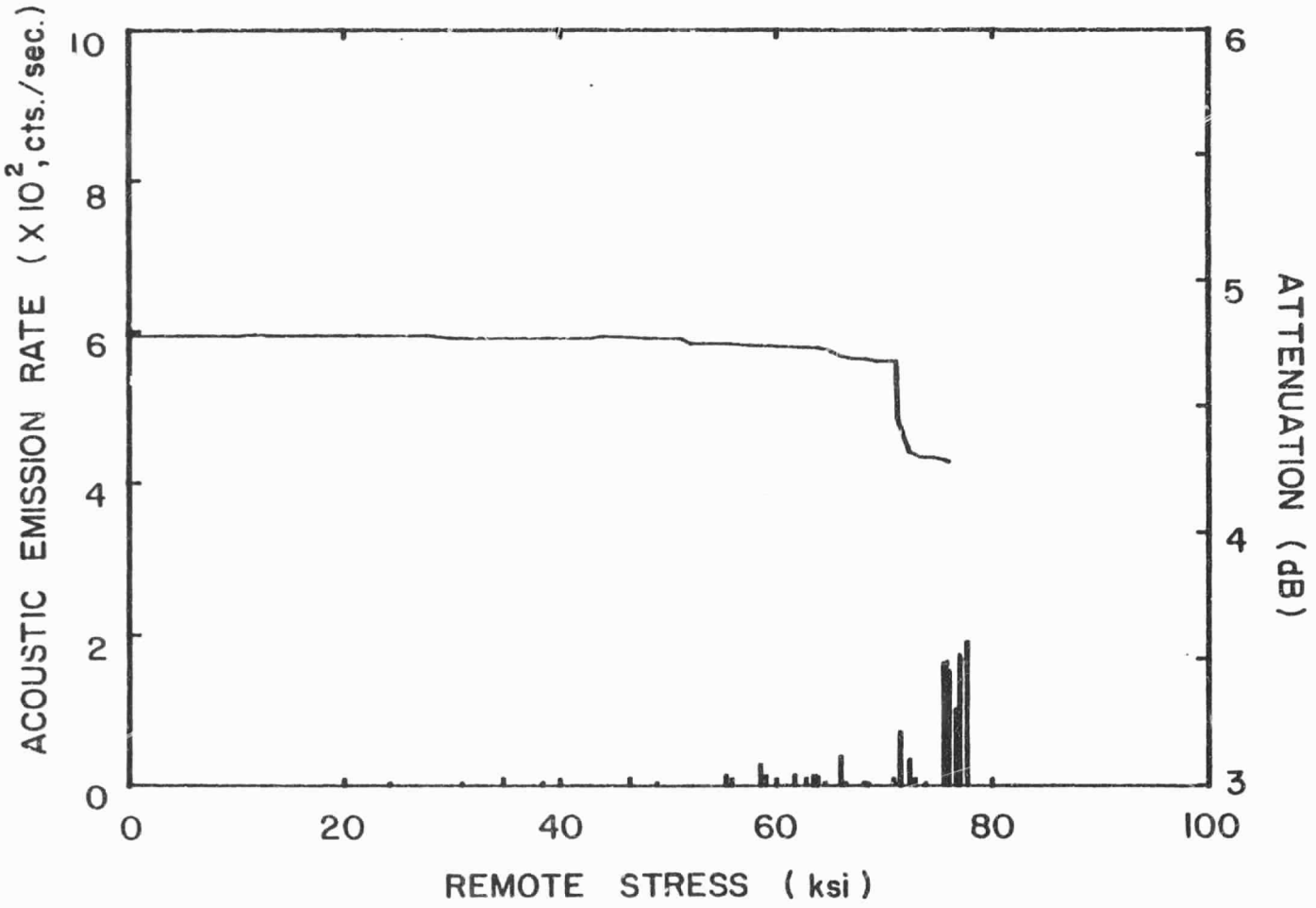

Fig. 7. Acoustic emission rate and attenuation vs. applied stress for a $[\pm 45,0]_s$ specimen with a longitudinal flaw in the interior 0° plies loaded statically to failure.

in the unconstrained $[0]_6$ longitudinally notched specimens. The interior 0° ply stress was about 145 ksi (1000 MPa) for the biaxially constrained situation.

Fatigue Tests

Fatigue damage of the transversely notched $[0]_6$ (type 6) specimens initiated at the notch tips and propagated parallel to the fibers in an "H" pattern. The distance over which these axial cracks travelled varied in length, depending on the maximum load applied. For instance, when a type 6 specimen was cycled at a maximum stress amplitude of 50 percent of its static strength, axial splits developed at the crack tips as early as 2230 cycles, growing to approximately 1/2 inch in length by 3500 cycles. After 12,400 cycles of fatigue loading, the cracks had propagated to the gripped section. At high stresses, the cracks could propagate into the gripped region, causing a pull-out of the ligaments from the grips and a longitudinal failure. The crack initiation and growth during the fatigue loading could be easily followed by thermography although the hottest spot usually lagged slightly behind the travel of the tip of the crack.

A constrained notched 0° ply, such as in type 10 and type 14 specimens, presents a more complicated situation. The local stress field in the neighborhood of the flaw is extremely complex. The orientation of the constraining plies and the interlaminar stresses present influence the damage development around the embedded flaw in many ways. A three-dimensional analysis of the stress field in the neighborhood of a crack in an interior lamina in a laminate had been undertaken and will be discussed in a later section.

C-scan Results

C-scan histories of specimens with embedded flaws are presented in Figs. 8-15. The c-scans were made at the cyclic intervals shown in the figures. In all figures, the horizontal arrow locates the position of the embedded flaw.

Figure 8 shows the development of damage as revealed by c-scans of a type 10 $[90/0]_s$ specimen after 100k, 300k, and 700k cycles at an applied stress equal to 36 percent of UTS. By 100k cycles, and "H" pattern has formed at the flaw. Sectioning studies, described in section II of the report, show that the damage consists of axial cracks at the tips of the notch in the 0° plies and delamination of the 90/0 interface. In addition, transverse cracks in the 90° constraining plies are also present. Additional cycles at this stress level cause the damage zone to grow in the transverse direction. Between 300k and 700k cycles, the c-scan reveals little or no growth of the damage zone. All c-scans in this report are made by gating on the same echo and using the same sensitivity so that the size of the defective zones in different c-scans can be directly compared and used as a relative measure of the size of the damage zone detectable by the ultrasonic c-scan technique.

Higher applied stresses produce higher damage zone growth rates and larger damage zones. Figure 9 shows that the damage zone in a type 10 $(90/0]_s$ specimen at 51 percent of UTS continues to grow in the axial direction during the first 100k cycles where the test was stopped and the specimen was sectioned. However, the transverse growth of the damage zone stopped after 5k cycles. Thermographs recorded during this test show "H" shaped hot spots as early as 1k cycles. Figure 10 shows that after 100k cycles at 70 percent UTS, the damage has extended to the

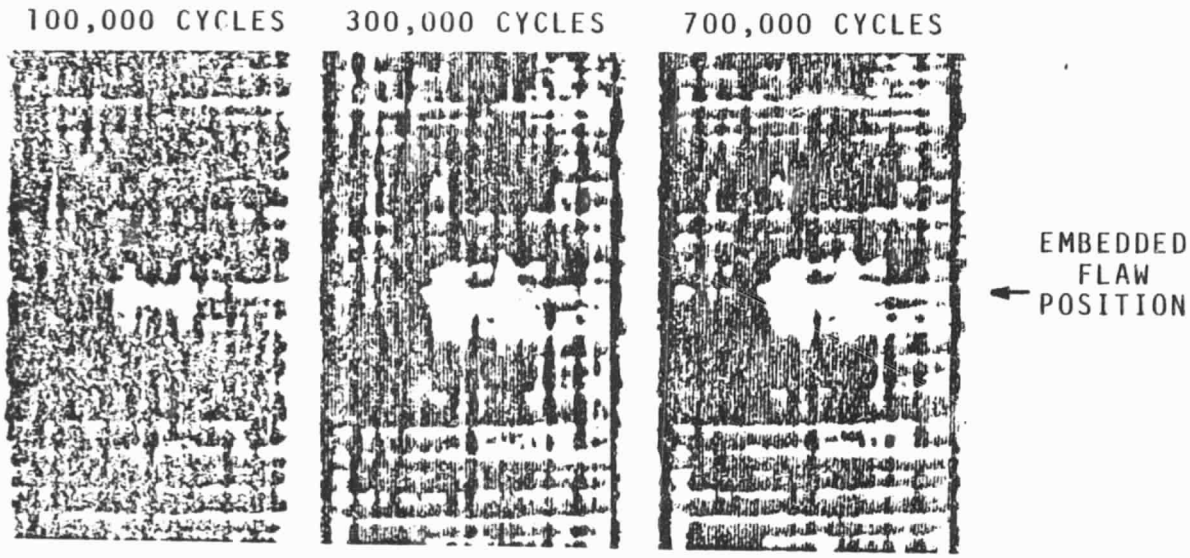

Fig. 8. C-scan history of a type 10 $[90,0]_s$ laminate with a notch embedded in the interior 0° plies under cyclic loading at 36% UTS. The nominal stress in the 0° plies is 70% of the notched tensile strength of type 6 specimens.

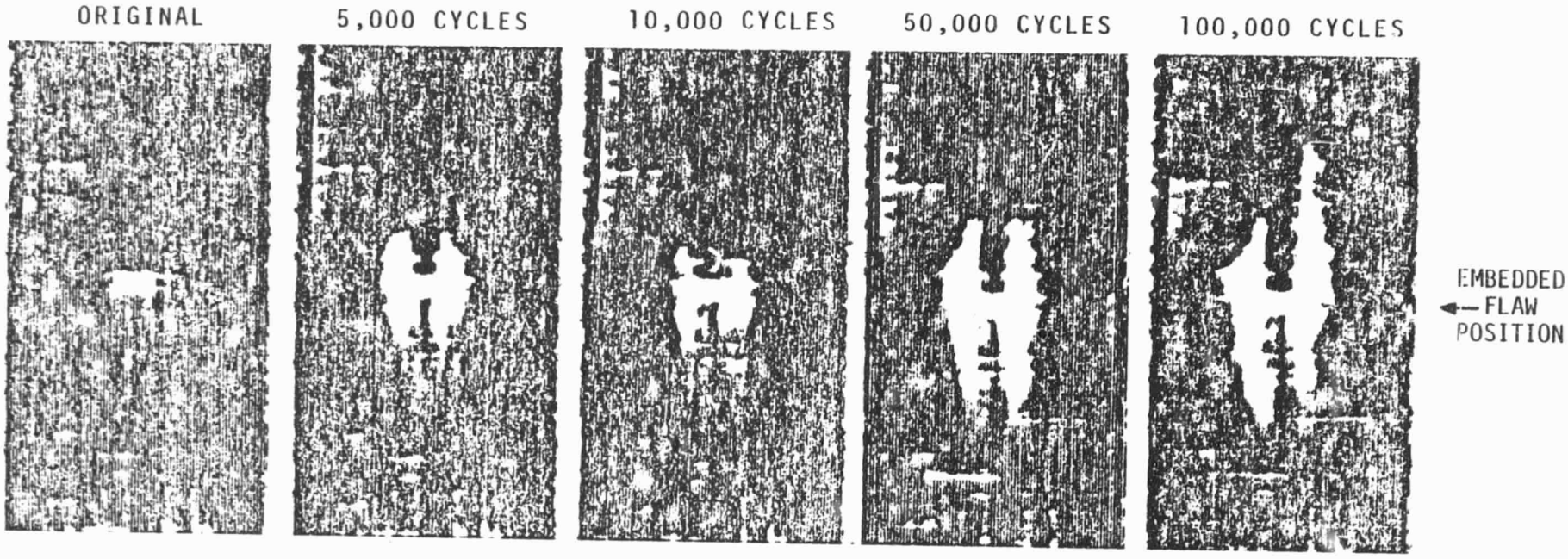

Fig. 9. C-scan history of a type 10 $[90,0]_s$ laminate with a notch embedded in the interior 0° plies under cyclic loading at 51% UTS. The nominal axial stress in the 0° plies is 100% of the notched tensile strength of type 6 specimens.

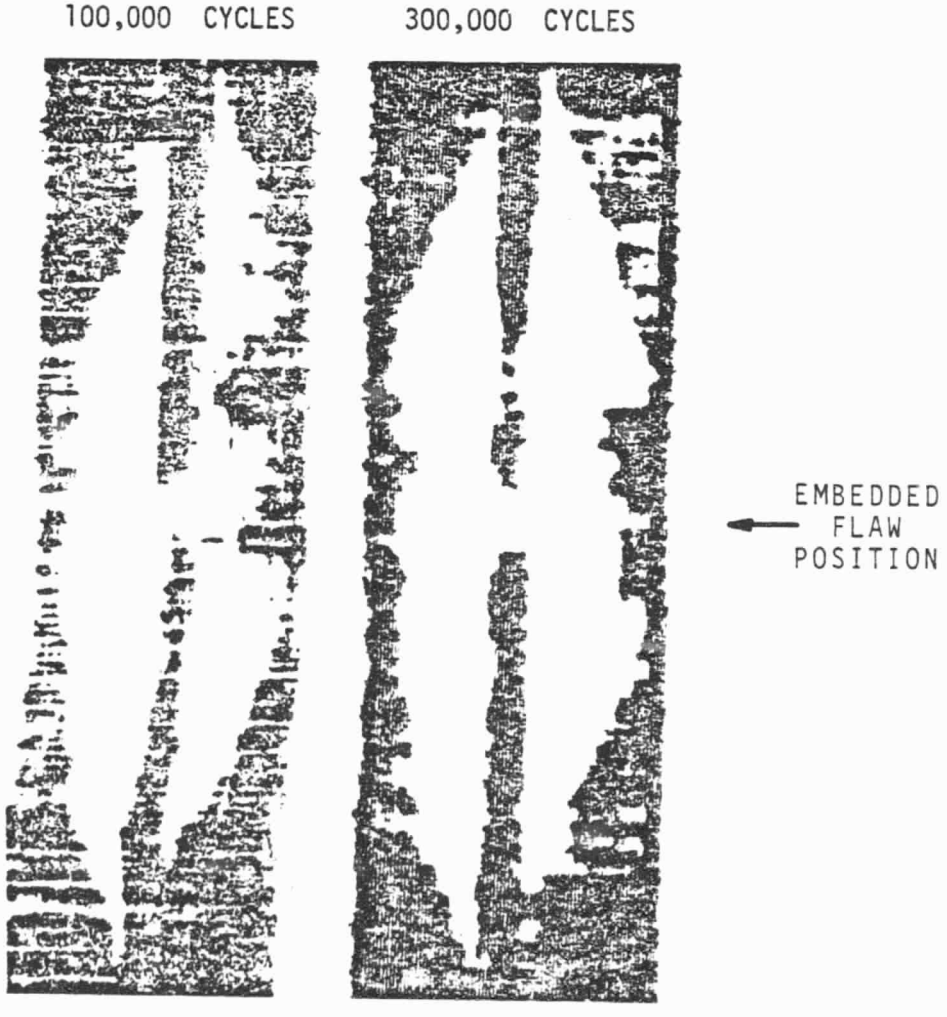

Fig.10. C-scan history of a type 10 [90,0]$_s$ laminate with a notch embedded in the interior 0° plies under cyclic loading at 70% UTS. The nominal stress in the 0° plies is 134% of the notched tensile strength of type 6 specimens.

grips in the axial direction and additional cycling to 300k cycles increases the extent of the damage in the transverse direction. By 300k cycles, the 90/0 interfaces had delaminated to the extent that the 90° plies no longer were effective constraining plies and the test was stopped. Visual inspection showed that the four axial cracks extending from the notch tips in the 0° plies had grown into the grip region creating a "no load" strip of unidirectional material above and below the embedded flaw and two load carrying strips on each side of the flaw.

Damages zones in type 14 $[\pm 45/0]_s$ laminates are shown in Figs. 11 and 12. The c-scans in Fig. 11 show the defective region around an embedded flaw in a specimen cycled at a maximum stress of 41 percent UTS. By 100k cycles, a damage zone has developed in the flawed region; however, there appears to be little or no growth of the zone after 310k cycles. During this test, the thermographic camera detected a hot spot as early as 3.3k cycles, although the thermographic pattern was not as distinct as in the type 10 laminates.

Increasing the applied stress to 63 percent UTS creates a larger damage zone after 100k cycles than does cycling at 41 percent UTS. The higher stress also causes the damage zone to increase in size between 5k and 100k cycles. The thermographs recorded a hot spot in the flawed region by 1.1k cycles.

Some of the effects of the orientation of the constraining plies can be seen in Figs. 13 and 14. Figure 13 compares the c-scans of a type 10 $[90/0]_s$ laminate with a type 14 $[\pm 45/0]_s$ laminate after 100k cycles. The applied maximum stress is such that the nominal maximum stress in the 0° plies is equal to 70 percent of the tensile strength of

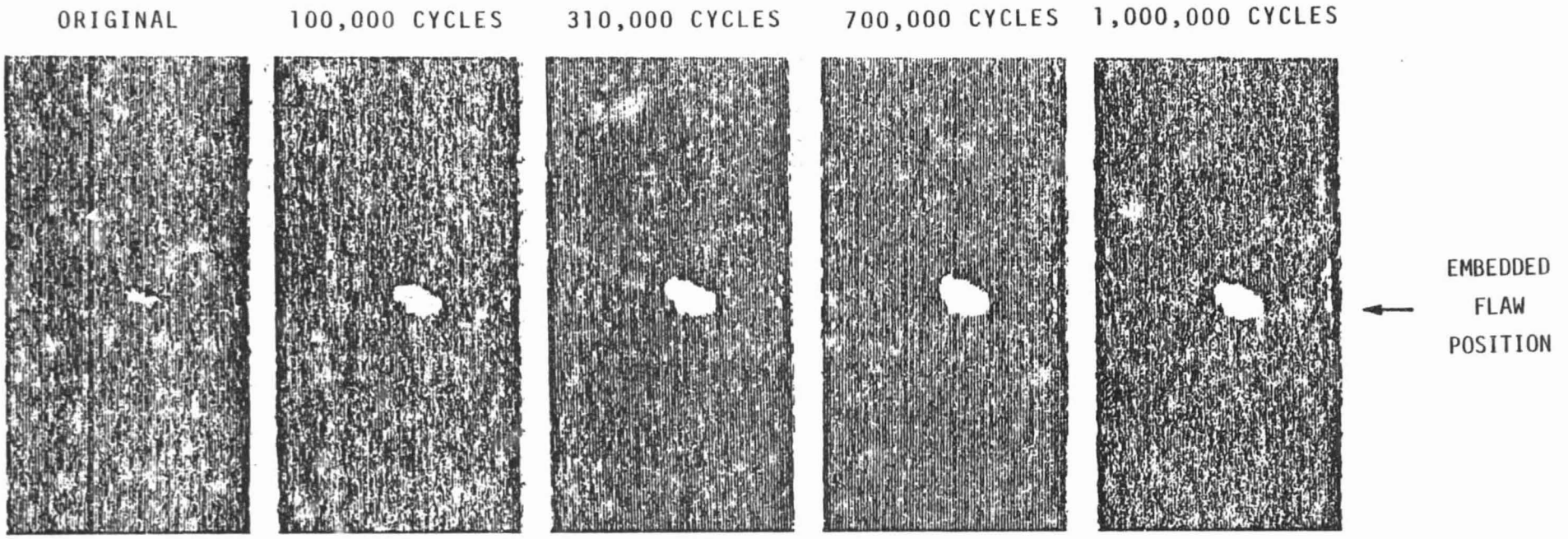

Fig. 11. C-scan history of a type 14 $[\pm 45,0]_s$ laminate with a notch embedded in the interior 0° plies under cyclic loading at 41% UTS. The nominal stress in the 0° plies is 70% of the notched tensile strength of type 6 specimens.

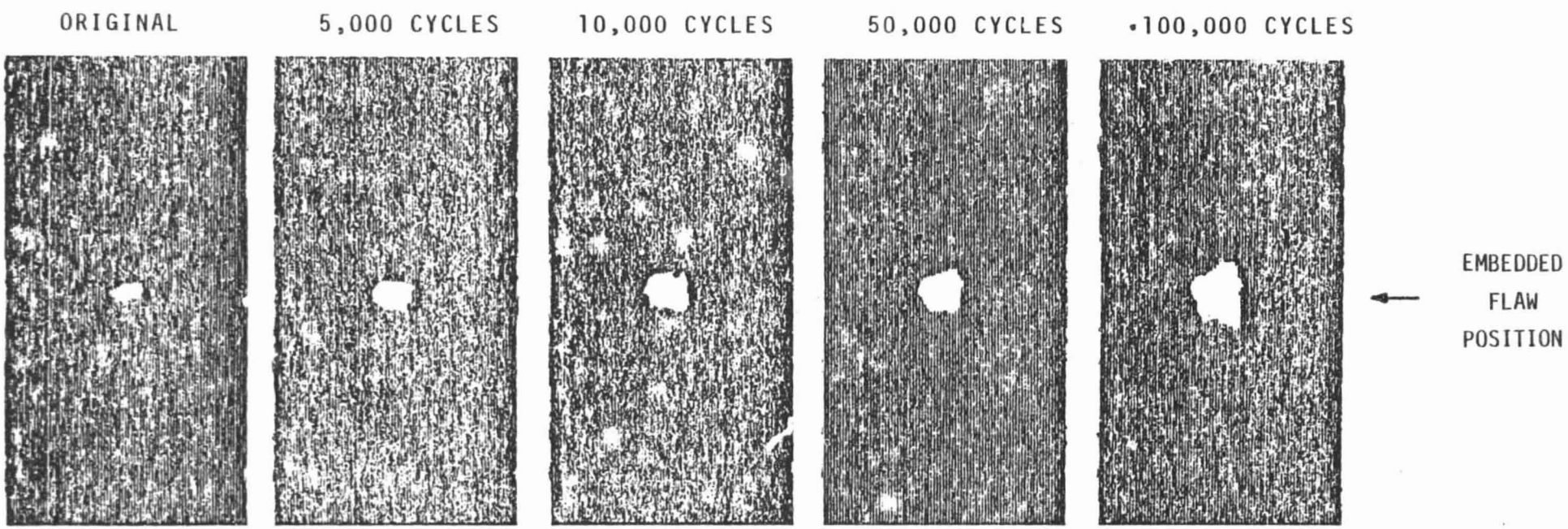

Fig.12. C-scan history of a type 14 $[\pm 45,0]_s$ laminate with a notch embedded in the interior 0° plies under cyclic loading at 63% UTS. The nominal axial stress in the 0° plies is 100% of the notched tensile strength of type 6 specimens.

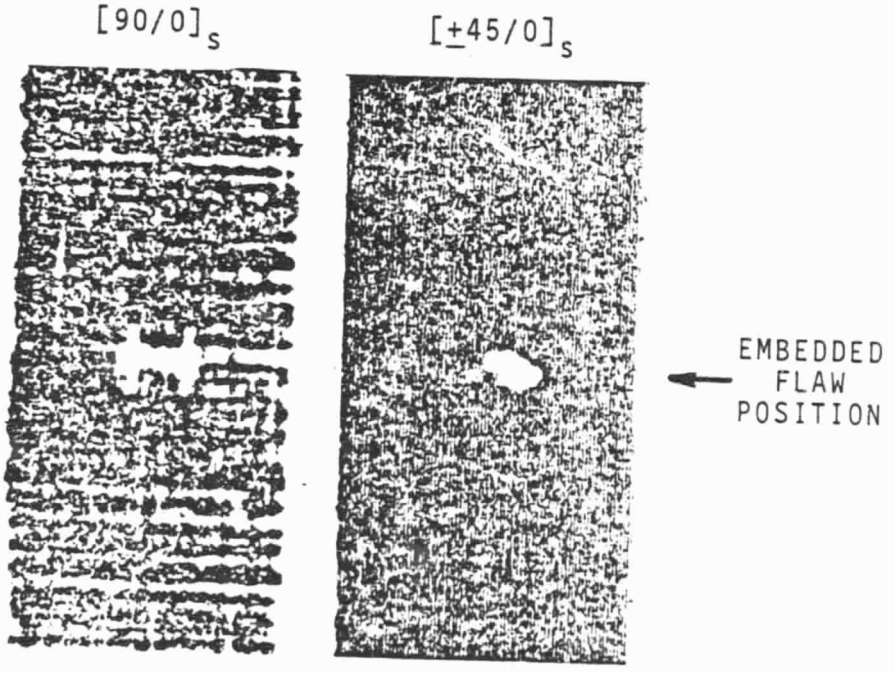

Fig.13. Ultrasonic c-scans of a type 10 $[90,0]_s$ and a type 14 $[\pm 45,0]_s$ laminate after 100,000 cycles of fatigue loading. In each case, the nominal axial stress in the interior 0° plies is 70% of the notched tensile strength of type 6 specimens.

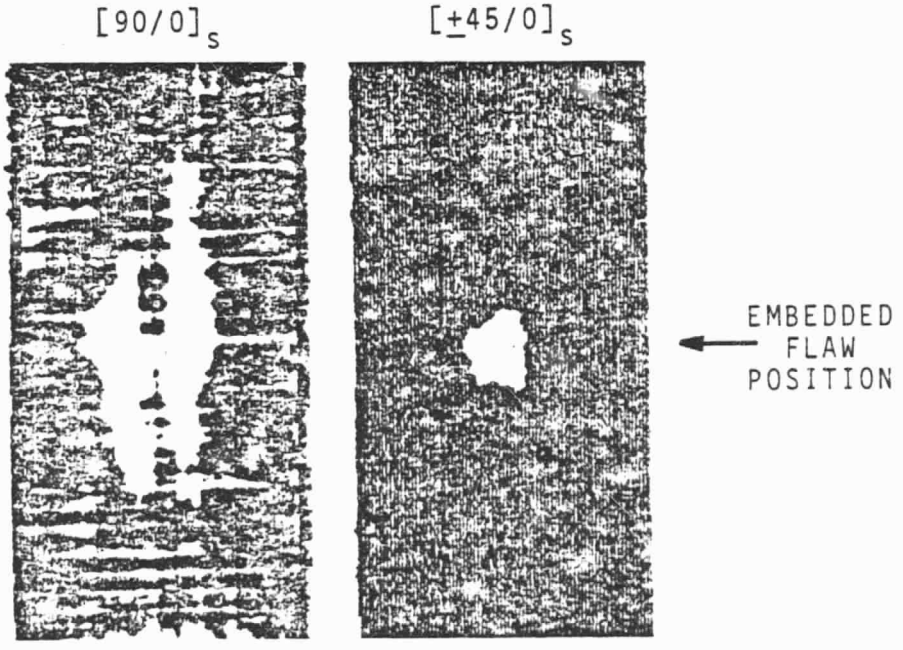

Fig.14. Ultrasonic c-scans of a type 10 $[90,0]_s$ and a type 14 $[\pm 45,0]_s$ laminate after 100,000 cycles of fatigue loading. In each case, the nominal axial stress in the interior 0° plies is 100% of the notched tensile strength of type 6 specimens.

0° unidirectional laminates with a center notch (type 6 specimens). The damage zone in the $[90/0]_s$ specimen has the "H" shape mentioned previously with damage regions extending away from the notch tips in the 0° direction. This c-scan also shows defective areas throughout the $[90/0]_s$ specimen whereas the defective region is confined to the flaw area in the $[\pm45/0]_s$ specimen. Visual observation of the $[90/0]_s$ specimen shows that these defects are delaminations of the 90/0 interface which allow the exterior 90° ply to peel off. The area of the horizontal bar in the "H" pattern is approximately equal to the area of the damage zone in the $[\pm45/0]_s$ specimen. At applied stresses such that the 0° ply stress is equal to the notched tensile strength of unidirectional specimens, the damage zone in the $[90/0]_s$ specimen is much larger than in the $[\pm45/0]_s$ specimen after the same number of cycles, Fig. 14. The "H" pattern is extended toward the grip region; however, the damage zone in the $[\pm45/0]_s$ specimen is again confined to the embedded flaw region.

When the orientation of the embedded flaw in the 0° plies is parallel to the fiber direction as in type 15 and 16 specimens, the influence on the damage growth by the orientation of the constraining plies is greatly reduced. Figure 15 shows the c-scans of a $[90/0]_s$ and a $[\pm45/0]_s$ longitudinally flawed specimen after 100k cycles of fatigue loading. The nominal maximum stress in the 0° plies is approximately equal to 69 percent of the tensile strength of 0° unidirectional laminates with a center longitudinal notch (type 5 specimens). The damage growth for these specimens was slow but gradual. Although the $[\pm45/0]_s$ exhibited a greater degree of delamination after 100k cycles, the development of fatigue damage for this flaw orientation was quite localized for both

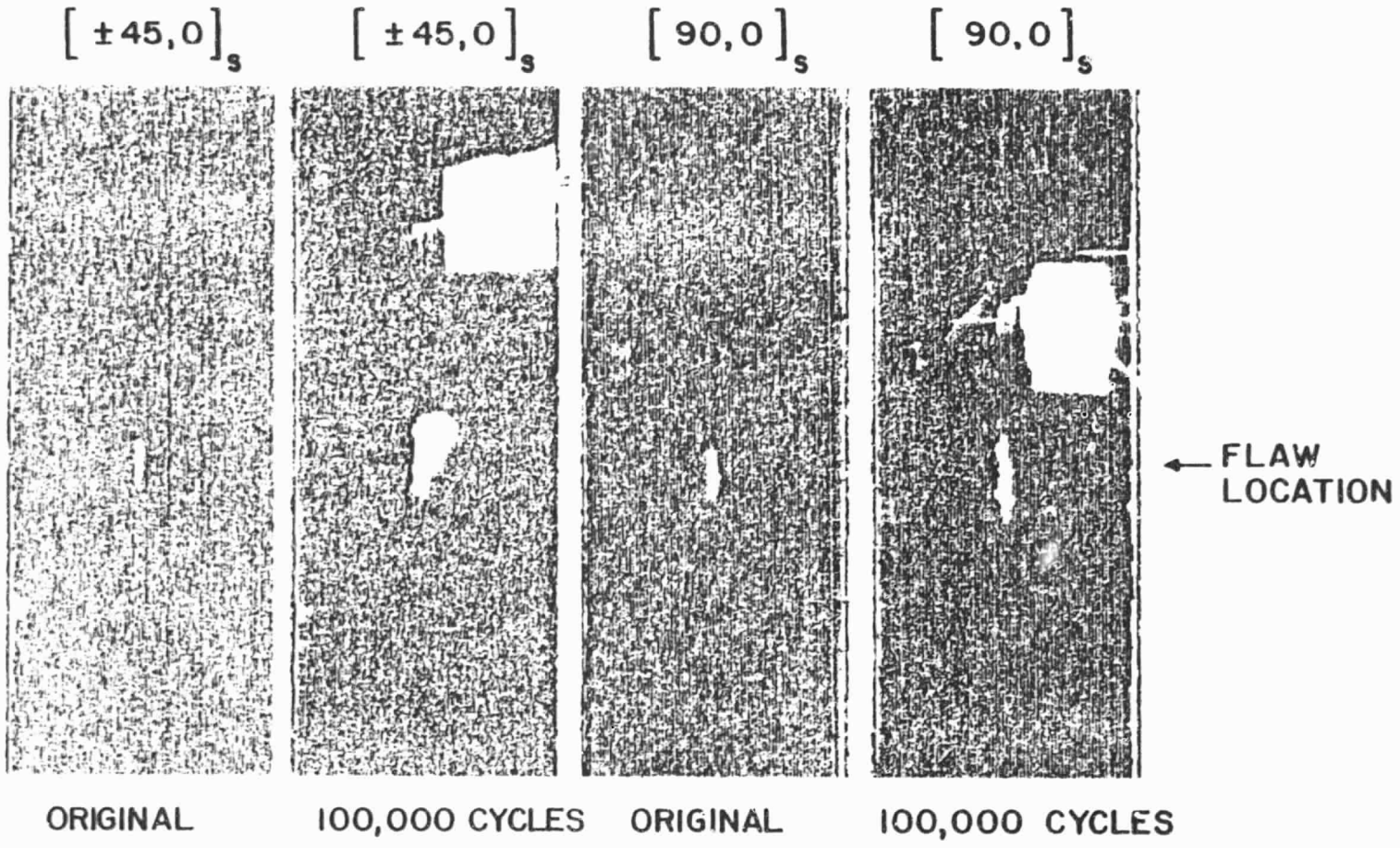

Fig. 15. Ultrasonic c-scans of longitudinally flawed $[90,0]_s$ and $[\pm 45,0]_s$ specimens. In each case, the nominal axial stress in the interior 0° plies is 69% of the notched tensile strength of type 5 specimens.

orientations of constraining plies when compared to the transversely flawed specimens (Fig. 13).

X-Ray Results

The fatigue damage of laminates containing flawed interior 0° plies is a complex mechanism involving both axial splitting in the interior 0° plies and delamination at the interfaces. The question as to which of these occurs first remains unanswered thus far. One way to better understand the situation is to determine the extent of propagation of these axial cracks in the interior 0° plies.

As mentioned earlier in the sectioning studies, the ultrasonic c-scans give a 2-D view of the delaminated surfaces. The extent of axial splitting depends on the orientation of the constraining plies. In the case of a transversely flawed specimen, the axial splits are confined to the delaminated region for the $[\pm 45/0]_s$ case, but extend beyond the delaminated region when the constraining plies are 90° plies. X-ray radiographs were taken of some of these specimens in an attempt to follow the development of the axial cracks.

Figure 16 shows the x-ray and c-scan history of a type 10 specimen after 105k cycles of fatigue loading. The maximum nominal stress in the 0° plies is 100 percent of the notch strength of the type 6 specimens. The arrows in the diagram represent the tips of the axial splits as detected by the x-ray. In all cases, the extent of the splitting exceeds the delaminated area shown by the c-scans, although the general shapes of the damaged region correlate well with one another.

Stiffness

The percent change in the apparent stiffness measured by a clip

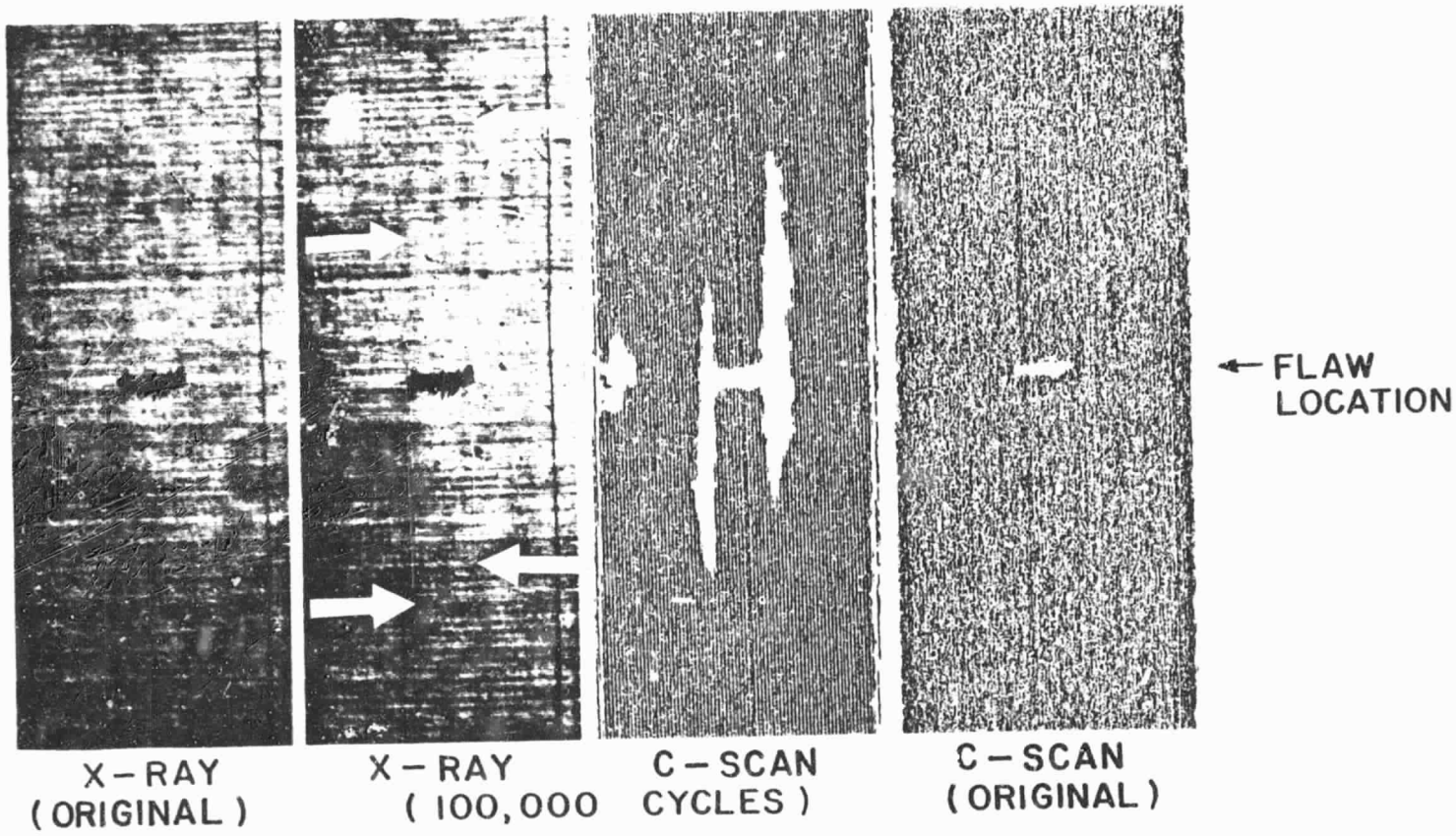

Fig.16. X-ray radiographs and ultrasonic c-scans of a type 10 ($[90,0]_s$ laminate with a transverse flaw in the interior 0° plies) specimen after 100,000 cycles of fatigue loading. The nominal axial stress in the 0° plies is 100% of the notched tensile strength of type 6 specimens.

gauge across the embedded flaw region of the specimens can be related to the damage growth in the laminates. Figures 17 and 18 show the changes in the apparent stiffness of the $[90/0]_s$ and the $[\pm 45/0]_s$ flawed laminates respectively. In both cases, the percent change depends upon the stress amplitude and the number of cycles of fatigue loading, which govern the damage present and the growth of damage under cyclic loading. For specimens where the c-scans indicate a large degree of delamination, there is usually a significant decrease in the apparent stiffness measured at the corresponding life cycle.

The effect of the orientation of the constraining plies on the damage growth can be reflected by a comparison of the stiffness changes in these specimens (Fig. 19). The two specimens with nominal 0° ply stresses equal to 70 percent of the notched unidirectional tensile strength (type 10, 36 percent UTS and type 14, 41 percent UTS) suffer the same percent degradation of stiffness during the first 300k cycles, after which the stiffness of the $[\pm 45/0]_s$ specimen remains constant and the stiffness of the $[90/0]_s$ specimen continues to decrease. At nominal 0° ply stresses equal to the notched strength of unidirectional specimens, the percent stiffness change is greater in the 51 percent UTS type 10 specimen than in the 63 percent UTS type 14 specimen. Again, the stiffness of the $[\pm 45/0]_s$ specimen initially decreases and remains constant whereas the stiffness of the $[90/0]_s$ specimen continues to decrease for 100k cycles. At 70 percent UTS, the damage in the $[90/0]_s$ specimen extended to the grips by 100k cycles with a corresponding stiffness decrease of 70 percent. As the damage continued to spread across the width of the specimen the stiffness also continued to decrease.

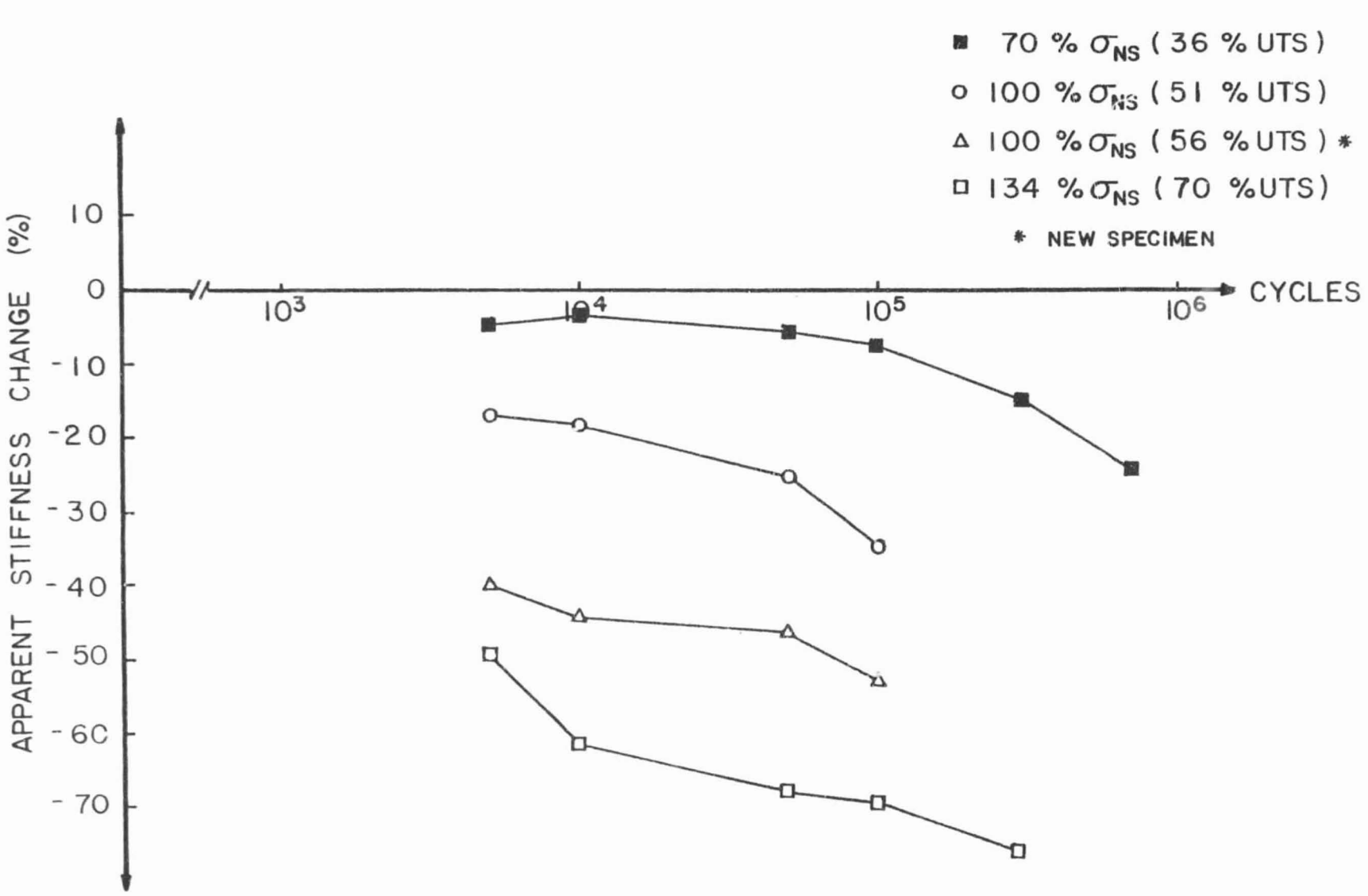

Fig. 17. Changes in the apparent stiffness across the flawed region for type 10 ($[90,0]_s$ with a transverse flaw in the interior 0° plies) specimens during fatigue loading.

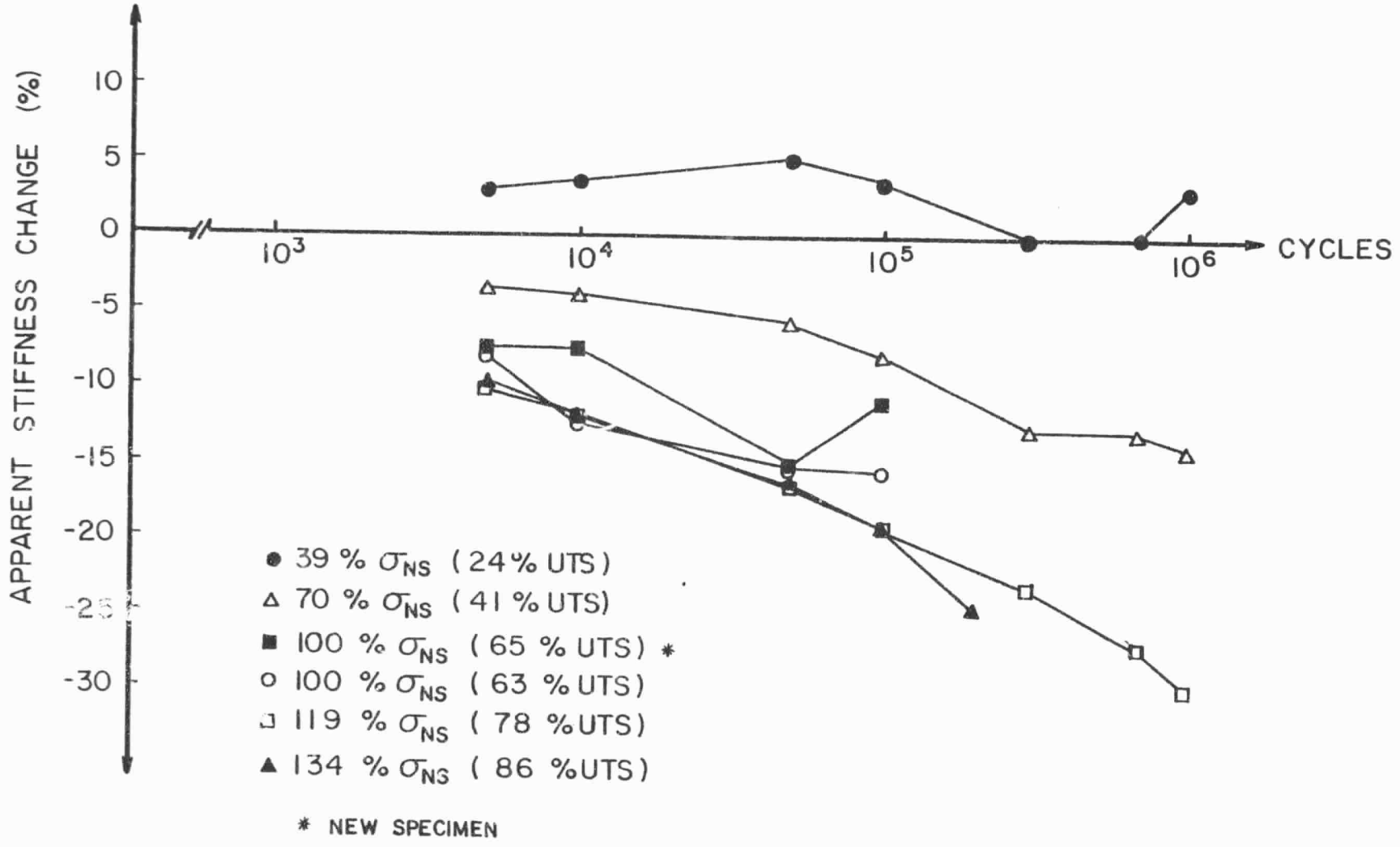

Fig. 18. Changes in the apparent stiffness across the flawed region for type 14 ($[\pm 45,0]_s$ with a transverse flaw in the interior 0° plies) specimens during fatigue loading.

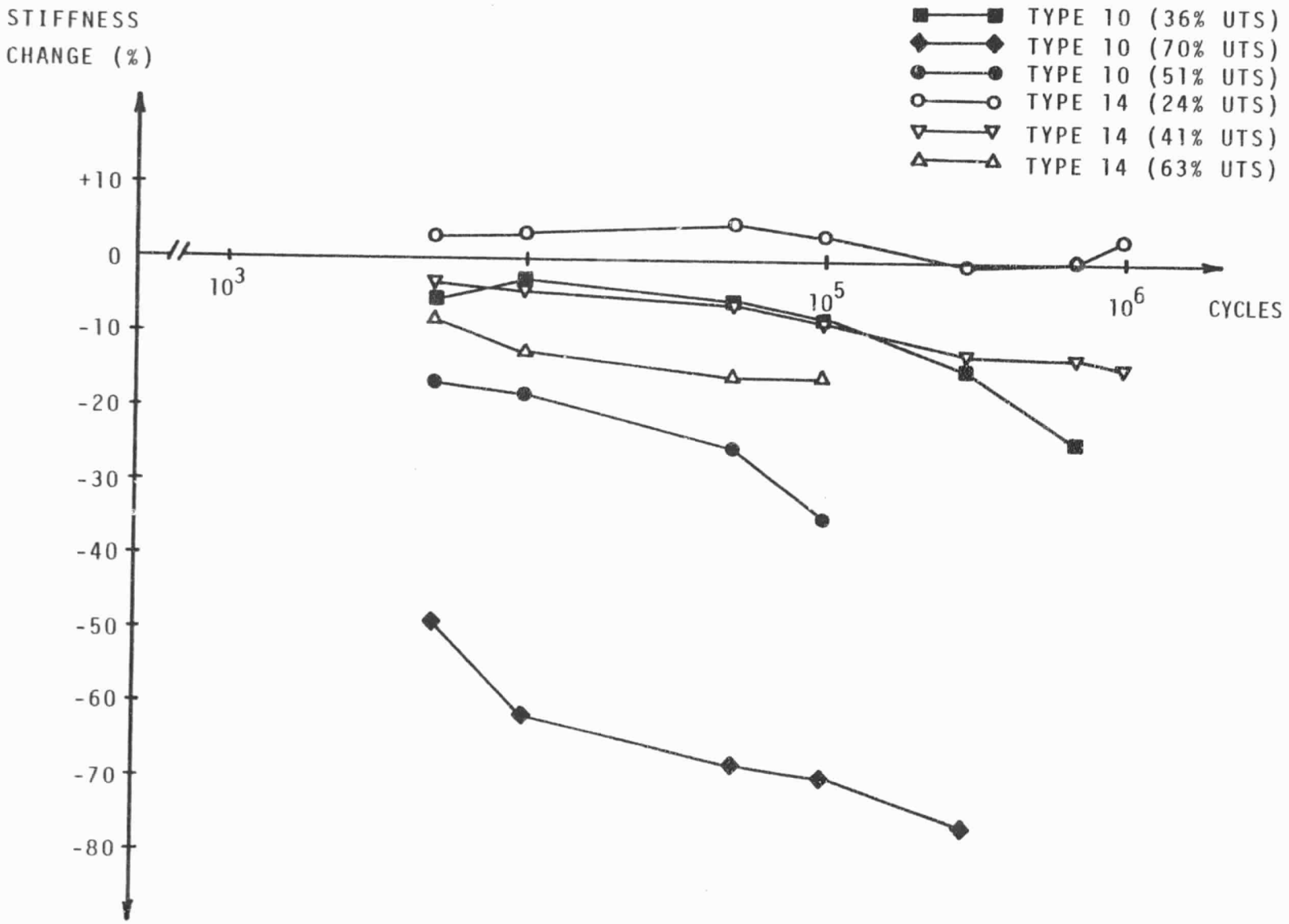

Fig.19. Changes in the apparent stiffness across the flawed region of type 10 ($[90,0]_s$ with embedded flaw) and type 14 ($[\pm 45,0]_s$ with embedded flaw) specimens during cyclic loading.

Residual Strength

In the previous sections, the discussion of the fatigue damage in the transversely flawed laminates (type 10 and type 14 specimens) is usually described in terms of three measurable parameters: namely, the extent of axial cracking in the interior 0° plies; the degree of delamination at the interfaces; and the decrease in the apparent stiffness in the global section of the flawed region. Table III lists the residual strength data for some of the specimens which had undergone various cycles of fatigue loading at some predetermined cyclic stress amplitude, such that the extent of fatigue damage in these specimens is distinctly different. For instance, for the type 10 specimens, in specimen number 4, the damage in the laminate was severe, with the axial cracks at the flaw tips running all the way into the grip region and massive delamination along the axial cracks. Specimen number 2 contained only a small degree of axial splitting with some localized delamination. The damage in specimen number 3 was similar to that of number 2, but the travel of the internal axial cracks was longer.

When these specimens were pulled for residual strength after cyclic loading, there was very little difference in the final fracture mode. The failure mode was a transverse fracture with some degree of axial cracking in the interior 0° plies both at the tips of the flaw and in the remote region, and is quite similar to the static failure mode of the specimens which had not undergone cyclic loading. There is no apparent difference in the residual strengths of these specimens, and in all cases, the net section stress in the interior 0° plies at fracture exceeds the measured strength of the unnotched unidirectional 0° laminates (type 1) of 142 ksi (980 MPa). In the case of specimen number 4,

TABLE III RESIDUAL STRENGTH DATA FOR TYPE 10 AND TYPE 14 SPECIMENS

SPECIMEN TYPE AND NUMBER	LOAD HISTORY (CYCLES @ STRESS)	AVERAGE TENSILE STRENGTH OF SPECIMEN TYPE (KSI)	RESIDUAL STRENGTH AFTER FATIGUE LOADING (KSI)	NET SECTION STRESS IN 0° PLIES AT FAILURE (KSI)	
				STATIC (average)	RESIDUAL
10 $[90/0]_s$#1	38K @ 120%σ_{NS}	82	72.34	164	156
10 $[90/0]_s$#2	100K @ 100%σ_{NS}	82	82.1	164	163
10 $[90/0]_s$#3	10^6 @ 100%σ_{NS}	82	84.88	164	168
10 $[90/0]_s$#4	10^6 @ 130%σ_{NS}	82	91.33	164	172
14 $[\pm45/0]_s$#1	10^6 @ 120%σ_{NS}	51	57.21	136	148
14 $[\pm45/0]_s$#2	100K @ 100%σ_{NS}	51	45.82	136	120
14 $[\pm45/0]_s$#3	10^6 @ 100%σ_{NS}	51	47.95	136	122

the degree of axial splitting was more severe and there was evidence of multiple transverse fractures in the 0° plies, resulting in a higher strength value.

Similar results were obtained for the type 14 specimens. Here, since the biaxial constraining plies restrict the spread of the fatigue damage, the final damage states in the specimens are not significantly different. The net section stress at failure in the 0° plies was lower than the average static value and the strength of the unnotched unidirectional 0° specimens suggesting that the influence of the notch is still present.

DISCUSSION AND INTERPRETATIONS:

The general objective of this investigation was to achieve an understanding and representation of constraint effects for a well controlled set of circumstances. The motivation for such an undertaking is provided, primarily, by the possibility of reaching a level of understanding which is sufficient to support the accurate anticipation of unfamiliar situations involving constraint effects. For that reason we have tried to classify and catagorize our observations as precisely as possible, and have attempted to develop concepts that are more general than our specific observations. This section is devoted to that aspect of our work. While our comments must be viewed as present opinions based on our past experience and the present investigation, in every case our remarks are supported by facts. Since all such facts are not yet available, the "generalities" which can be drawn are "general" in that context, a common situation.

The approach we used in our investigation, as described earlier, will be the approach we use in our attempt to rationalize the results. Specifically, we believe that a workable logic can best be constructed based on the last ply to break — the zero degree (0°) plies in our discussion below. The approach consists of evaluating constraint effects as they influence the behavior of the controlling plies. Hence, the behavior of the 0° plies alone is assessed, and the effect of adding various angle plies to the laminate is treated as the "constraint effect." The object of this rigor is the determination of strength, stiffness, or life of a laminate, or combinations of those, based on lamina response and rational analysis. The importance of such a capability for creative

design and efficient design can hardly be overstated.

It would appear that constraint effects, as we have defined them above, can be classified in two catagories, in-plane effects and through-the-thickness effects. The in-plane effects are those which act in the plane of the laminae and laminate, the (x,y) plane described earlier. Through-the-thickness effects can be thought of as occurring in the (x,z) plane which includes the through-the-thickness dimension of the laminae and laminate as well as the longitudinal (x) direction. The manner in which these two catagories effect response is fairly distinct in many regards, and the nature of the mechanics involved in the two cases is rather different. The in-plane problem involves a plane of uniform material properties so that linear elastic stress fields can be superposed. The in-plane response and the in-plane constraint effects are the principal contributors to notched strength (and changes in notched strength) under quasi-static loading. Through-the-thickness effects involve laminae boundaries. The stress fields in each lamina are coupled to those in the other laminae by interlaminar stresses. This material nonuniformity has a major influence on the effect of constraint and on the constraint stresses themselves (which are the interlaminar stresses). The major effect of through-the-thickness constraint stresses is on fatigue response; quasi-static notched response is influenced by the transfer of shear behavior across the boundaries of the 0° ply in regions above and below the notch but the shear that is being transferred is an in-plane shear. Through-the-thickness effects have more to do with delamination, longitudinal cracking and the growth and coupling of transverse cracks in the off-axis plies. These items

are more important to fatigue response than to quasi-static response.

We will begin by discussing the in-plane problem. To address that problem properly we define, more precisely, constraint effects. The interpretation is simple. If a lamina or laminae of identical type and orientation are unconstrained we assume we are discussing unidirectional behavior. If angle plies are laminated onto the 0° (or lowest angle) ply, they constrain the response of the unidirectional material accordingly. We consider that situation to define constraint effects. For the unnotched in-plane problem we can imagine the constraint process to be represented by Fig. 20. There a laminate consisting of 0°,45°, and 90° plies is shown at the top of the figure. When an axial (out of the paper) force is applied to the laminate the Poisson effect would cause the transverse dimensions (horizontal in the figure) to change in the proportions shown in Fig. 20b. (The thickness changes, which will be uniform, have been ignored.) Of course the laminae are bonded together so that the transverse strains shown in Fig. 20b are not allowed. Rather, each of the plies applies a transverse stress to its neighbor(s) so that a common transverse strain occurs as shown in Fig. 20c. The proportional magnitude of those transverse (constraint) stresses in also shown in Fig. 20c. For the present case the 0° plies are nearly "unconstrained" from the standpoint of the elastic stress state while the 45° and 90° plies experience large constraint stresses. The nature of the constraint is, of course, controlled by the orientation of the plies in a given laminate.

A list of unidirectional and laminate Poisson's ratios is shown in Table IV. The calculated values were determined from a laminate analysis. The Poisson contraction controls the magnitude of the constraint stresses

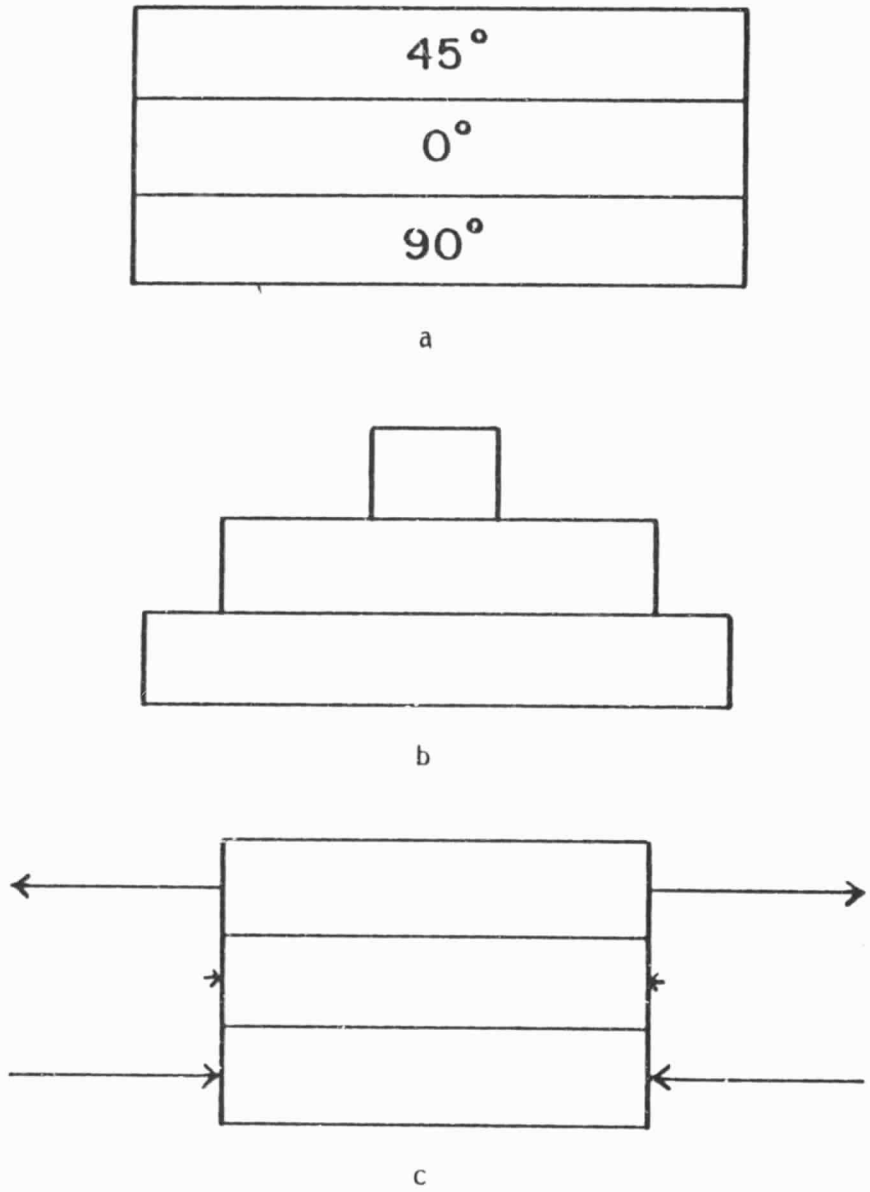

Fig. 20. Axial view of unloaded (a), loaded but unconstrained (b), and loaded and constrained (c) transverse (Poisson) displacement for a quasi-isotropic laminate under axial loading.

TABLE IV

POISSON RATIOS

Laminate	Measured Values	Calculated Values
$[0]_n$	0.29	---
$[90]_n$	0.031	---
$[\pm 45_n]_s$	0.78*	---
$[0,90]_s$	0.051	0.039
$[\pm 45,0]_s$	0.68	0.688
$[0,90,\pm 45]_s$	---	0.299

*from literature

and can be used to calculate the transverse (σ_y) component. While using engineering modulii, which are determined from unidirectional stress tests, is not a recommended general procedure for the determination of lamina stresses, the approximate value of the transverse stress (σ_y) can be quickly and easily obtained by a very simple procedure if Poisson's ratios are known. The most important aspect of the scheme is that it provides a conceptually simple rationale for understanding and mentally estimating the transverse normal stresses that are created by constraint. To apply the scheme one first calculates a "differential Poisson's ratio" defined as the absolute difference between the Poisson's ratio of the ply in question when that ply is unconstrained and the laminate Poisson's ratio when the subject ply is bonded into the laminate of interest. Analytically the expression is stated as

$$\Delta\nu = | \nu \text{ (constrained)} - \nu \text{ (unconstrained)} | \qquad \text{I}$$

For any given axial loading, represented by an axial strain of ϵ_x°, the "constraint effect" in the transverse direction is then given by

$$\Delta\nu\epsilon_x^\circ \qquad \text{II}$$

The transverse normal stress in the subject ply is then approximated by

$$\sigma_y^i = E_y^i \Delta\nu\epsilon_x^\circ \qquad \text{III}$$

where E_y^i is the engineering Young's modulus of the subject ply in the transverse (y) direction. The accuracy of such a simplified scheme is indicated by the comparisons shown in Table V. The "constraint stresses" shown there are σ_y stresses, and the "exact" values are those stresses calculated by a standard laminate analysis. The only noticeable difference in approximate and exact values is seen to occur for the $[\pm 45,0]_s$ laminate. The Poisson's ratio for 45° (or ±45°) laminae is not a well established

TABLE V

CONSTRAINT STRESSES

Constrained Ply	Exact	Approximate
0° ply in $[0,90]_s$	+ 1,418	+ 1,413
90° ply in $[0,90]_s$	− 1,418	− 1,399
0° ply in $[\pm 45,0]_s$	− 1,720	− 1,719
±45° plies in $[\pm 45,0]_s$	+ 860	+ 779 (ν=0.8)

number and may have contributed to the difference. In the context of our discussion it is especially important to notice the large difference in the constraint environment of the 0° plies in the two cases examined in Table V. In one case the σ_y constraint stress is positive and in the other case it is negative. (In both cases an axial strain of 1000 μ was applied to the laminate.) The transverse stress is significant in magnitude in both cases. It would be difficult to imagine that any damage that develops in the 0° plies would be unaffected by such a stress or that the nature of damage development in the 0° plies would be identical when the σ_y stress changes from a large positive to a large negative value. In fact, we have found that these stresses do have a significant influence on damage development. While some occasional suggestion of that fact has been made elsewhere from time to time, no damage growth model, that we are aware of, explicitly includes the influence of σ_y constraint stresses. In the case of unnotched response damage in the 0° plies consists, primarily, of longitudinal splitting along the 0° fibers in the unconstrained case. While final fracture requires transverse fiber breakage, the transverse fracture is nearly always discontinuous with regions separated by longitudinal splitting. The effect of transverse σ_y constraint stresses on this damage mode is easily noticed. For the $[0,90]_s$ laminate the transverse σ_y stress in the 0° ply is positive, as shown in Fig. 20. One might expect such a stress to contribute to an increase in longitudinal splitting, compared to the unconstrained behavior. It is, in fact, so. Our NDT results as well as our sectioning studies show a definite increase in the number of longitudinal cracks that form in the 0° plies for a given load or for a

given number of cycles at a given stress amplitude when the 90° plies are added to the unidirectional 0° plies. At the same time, adding the 45° plies to form the $[\pm 45,0]_s$ laminate, so that the transverse (σ_y) stress in the 0° plies is compressive, decreases the longitudinal splitting essentially to an unobservable level.

This situation is more complex but conceptually similar when a notch is present. Two basic modes of degradation at a notch in unidirectional orthotropic laminae are shown in Fig. 21. (Actually, the anisotropy is not an essential part of this discussion except as it changes the magnitude of the individual stress components.) In Fig. 21a the shear mode of damage is shown whereby a "plug" of material pulls out above and below the open crack surfaces by a shearing motion. The effect of constraint on this mode can also be seen by considering the superposition of the constraint stresses as we did for the unnotched case. The resistance to shear of the $[\pm 45,0]_s$ constrained case is nearly five times as great as the $[90,0]_s$ case. We might expect this damage mode to be very effectively suppressed in the $[\pm 45,0]_s$ laminate, and less so in the $[90,0]_s$ case. Precisely such a situation is observed in the laboratory. Figure 21b shows a second degradation mode whereby normal stresses develop across planes perpendicular to the crack and the crack plane, potentially causing a crack-opening mode of damage above and below the crack. This mode of damage is most influenced by the transverse (σ_y) in-plane constraint stresses discussed for the unnotched case. The nature of that effect for the present case is similar to the shear situation, i.e., the 45° plies superpose a compressive σ_y stress which tends to suppress the damage mode while the $[90,0]_s$ laminate has tensile σ_y stresses in the 0° plies, which should enhance longitudinal

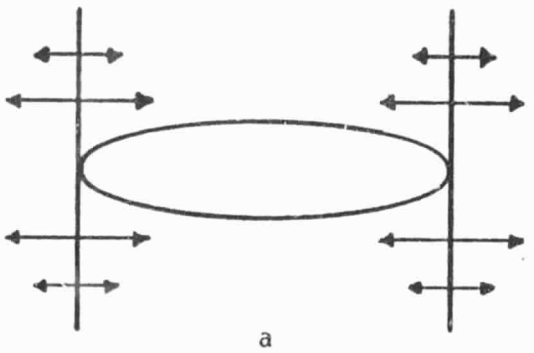

Fig. 21. Two basic modes of degradation at a notch in a unidirectional lamina.

crack formation and surface separation. Our investigation again confirms this behavior. It is interesting to note that the approximate models of damage growth and strength in the degraded condition do not account for the effect of the σ_y stress due to constraint, but the observations of physical behavior cannot be explained unless that component is included. For example, suppression of longitudinal cracking is usually ascribed to the superior shear resistance of the 45° plies. However, when a notch is not present, longitudinal cracking is enhanced (i.e., more longitudinal cracks form) when 90° plies are bonded to the unidirectional 0° plies. There are no in-plane shear stresses in that case; the only explanation is the tensile transverse normal stress induced by the constraint. One other point is important, regarding the details of our present constraint comparison. The $[\pm 45,0]_s$ laminate represents the "least damage" situation, i.e., the longitudinal cracking at the crack tip is very effectively suppressed in both the static and cyclic loading case. But that laminate does not have the greatest notched strength. The best way to compare strength, for the purposes of our discussion is to compare the net section (or nominal) stress in the 0° plies when failure occurs. All "strengths" will be calculated that way in this paragraph. The strength of the unidirectional 0° laminae was about 147 ksi (1014 MPa) in our tests. When a notch was added (transverse center notch) the strength dropped to 86 ksi (593 MPa). When the 90° plies were added to unidirectional 0° plies to form a $[90,0]_s$ laminate, the measured strength was 187 ksi (1289 MPa). When 45° plies were added to form the $[\pm 45,0]_s$ laminates the strength of the 0° plies became over 200 ksi (1379 MPa). The strength of the notched 0° plies constrained by 90° plies became 177 ksi (1220 MPa), which indicates that the notch

effect had essentially vanished. The notched strength of the $[\pm 45,0]_s$ laminate was about 145 ksi (1000 MPa) which shows some retention of the notch effect in this case where the notch geometry is retained by the constraint of the 45° plies. Hence, we see that the maximum constraint ($[90,0]_s$) does not correspond to the minimum damage, and the minimum damage ($[\pm 45,0]_s$) does not correspond to the maximum strength.

To summarize the in-plane effects, we must know the stress fields caused by the constraints. While this is generally not a major problem, good approximate schemes are difficult to construct and our understanding of post-damage stress states is incomplete. Equally important, we must know the dominant damage modes in the unconstrained and constrained case and how the constraint stresses affect those modes. Only when both of these situations are accurately assessed can the influence of constraint on strength, life and stiffness be correctly anticipated. If cyclic loading is present we must account for any new damage modes that result, especially the increased importance of interlaminar stresses and consequent debonding and delamination. Finally, we must account for interactions between damage modes and all constraint stresses, including the transverse normal stresses which seem to have been ignored in many modelling attempts.

The second general catagory of constraint effects is through-the-thickness effects. These effects are the result of interlaminar stresses that result from the different response of each lamina in the laminate. Two basic consequences of these stresses are most significant from the standpoint of influencing response. First, independent of the action of

an (in-plane) notch, the through-the-thickness constraint controls the pattern of transverse cracks that form in the off-axis plies of a laminate, which, in turn, controls the state of stress and state of strength of the laminate in the unnotched case. Second, the through-the-thickness stresses in the neighborhood of a notch (or transverse crack in a given lamina) control the tendency for delamination and crack growth along laminae boundaries. We will describe the first of these effects by a modelling exercise which follows.

The modelling method choosen was an equilibrium element approach similar to that which has been used by other authors for other fracture problems in composite materials [5,6]. A schematic of the idealized damage situation is shown in Fig. 22. In that figure, a crack is assumed to have formed in two plies having a total width "a". The schematic represents an edge view of the cracked laminate. We assume that the constraint layers next to the crack have an orientation of α degrees to the load axis. We further assume that the disturbance caused by the broken layer does not extend beyond the first constraining (unbroken) ply on either side of the broken ply. Finally, on the basis of experimental observations we estimate that any gradients in response from ply to ply occur over a distance, b, which extends for a distance of one twentieth of the ply width into each ply, or about the thickness of one tow or bundle on either side of the ply interface in the case of graphite epoxy for example. Actually, the analysis was tested by applying it to a special problem. We have observed that cracks that form in a single ply, or in adjacent plies of the same type, develop a regular spacing as loading (or the number of cycles of loading) is increased. It is our

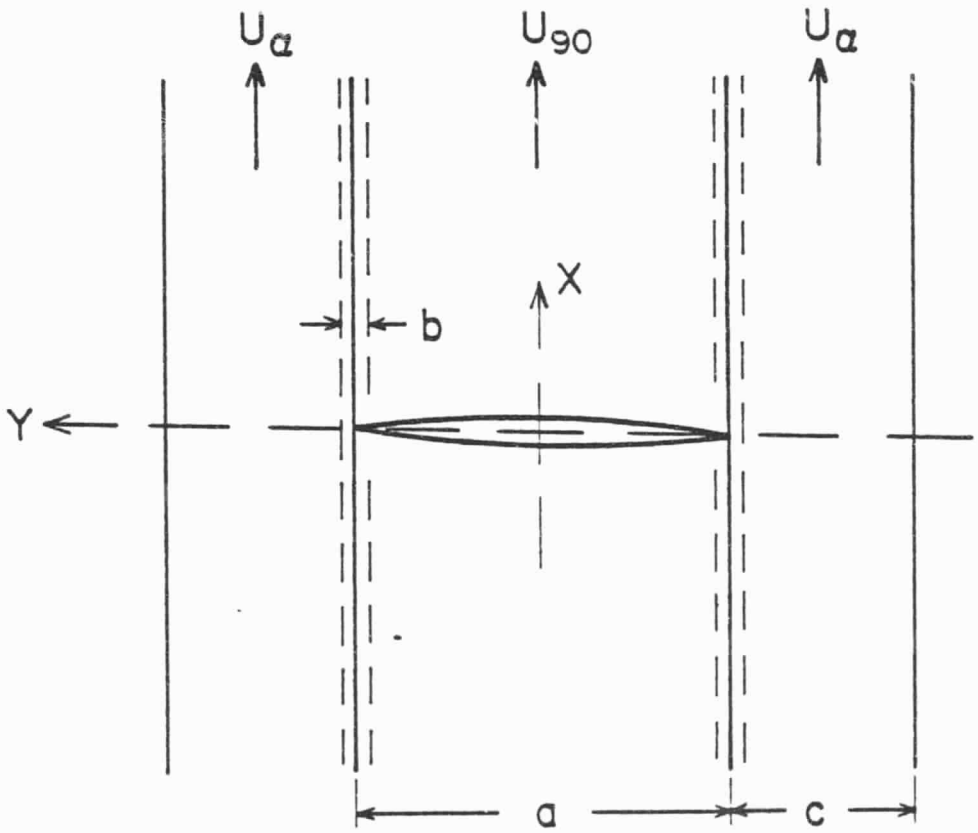

Fig. 22. Schematic diagram of a crack in two 90° plies at the edge of a laminate.

observation that this "saturation spacing," as we shall call it, is characteristic of specific laminates with specific stacking sequences and, as such, is an ideal test of our analysis. Five such cases were analyzed, as shown in Fig. 23. The analysis was used to predict the characteristic saturation spacing of cracks by assuming that the constraining layers transferred stress back into the broken ply on either side of the cracks until the stress which created the first crack was reached again. At that distance away from the first crack, a new crack will then form.

The results of the analysis are shown in Table VI, along with the spacing values measured experimentally. The experimentally determined values are expressed as the range of values included within one standard deviation above and below the average measured value. Both static and fatigue data are shown in one case.

The first two entries in Table VI show the results of calculated equilibrium spacings for a $[0,90]_s$ laminate and a $[90,0]_s$ laminate. The agreement between predicted and observed crack spacings is satisfactory. It is especially interesting to notice the large difference in crack spacing caused by only a change in stacking sequence, a clear indication of the importance of constraint effects. The $[0,90]_s$ laminates have nearly twice as many transverse cracks as the $[90,0]_s$ laminates in the 90° layers; the $[0,90]_s$ laminate also has the lowest quasi-static strength.

Crack spacings in a number of other situations are also shown in Table VI. In each case the constraint of each ply on its neighbors and of the laminate response on the individual plies determines the equilibrium crack spacing. Figure 24 shows a typical example of this equilibrium

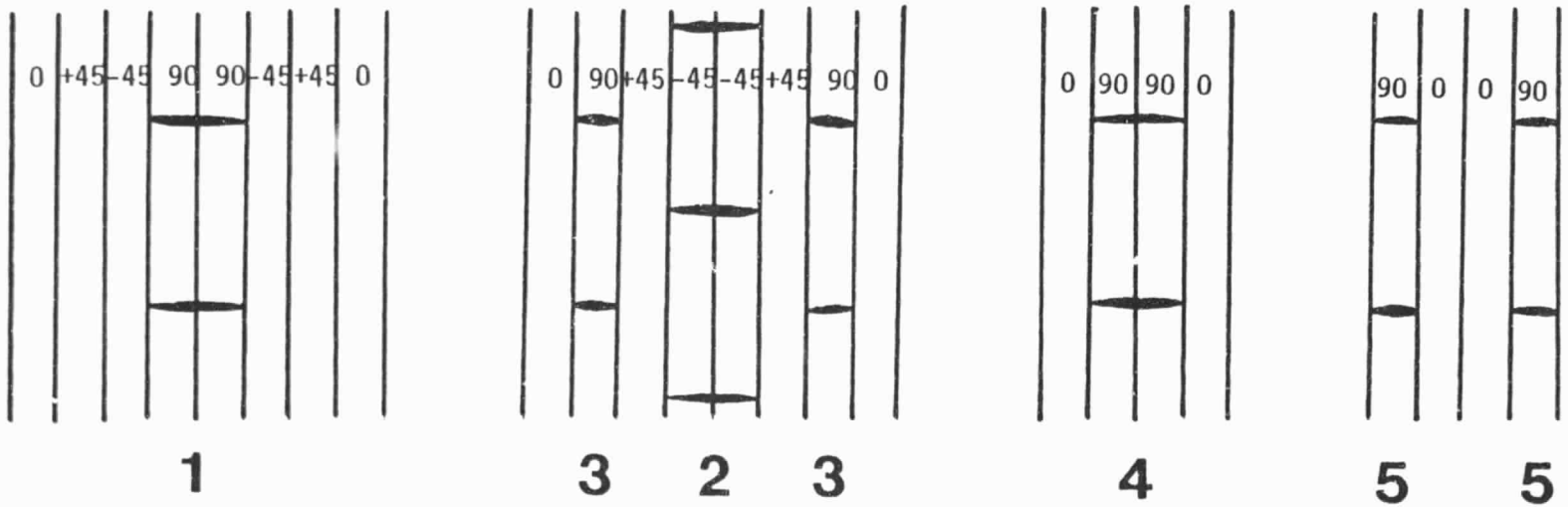

Fig. 23. Stacking sequences of laminates used in the prediction of saturation spacing.

TABLE VI

Specimen Type	Predicted Crack Spacing (mm)		Observed Crack Spacing (mm)
Cracks in two center 90° plies of $[0,90]_s$ laminate	0.882		1.087 - 0.532
Cracks in outside 90° plies of $[90,0]_s$ laminate	1.66		1.73 - 0.775
Cracks in center two 90° plies of $[0,\pm45,90]_s$ laminate	0.76	Static	1.51 - 0.62
	0.76	Fatigue	1.44 - 0.47
Cracks in two center 45° plies of $[0,90,\pm45]_s$ laminate	1.21		1.25 - 0.995
Cracks in single 90° plies of $[0,90\pm45]_s$ laminate	0.411		0.423 - 0.241
Cracks in +45° plies of $[0,90\pm45]_s$ laminate	0.875		0.909 - 0.524
Cracks in outside 90° plies of $[90_2,0,\pm45]_s$ laminate	1.12		1.40 - 1.07
Cracks in -45° plies of $[0,\pm45,90]_s$ laminate	0.879		0.960 - 0.889
Cracks in 90°_2 plies of $[0,90_2,\pm45]_s$ laminate	0.701		0.600 - 0.460
Cracks in +45° plies of $[0,90_2,\pm45]_s$ laminate	0.890		1.05 - 0.650
Cracks in -45° plies of $[0,90_2,\pm45]_s$ laminate	1.223		1.38 - 0.963

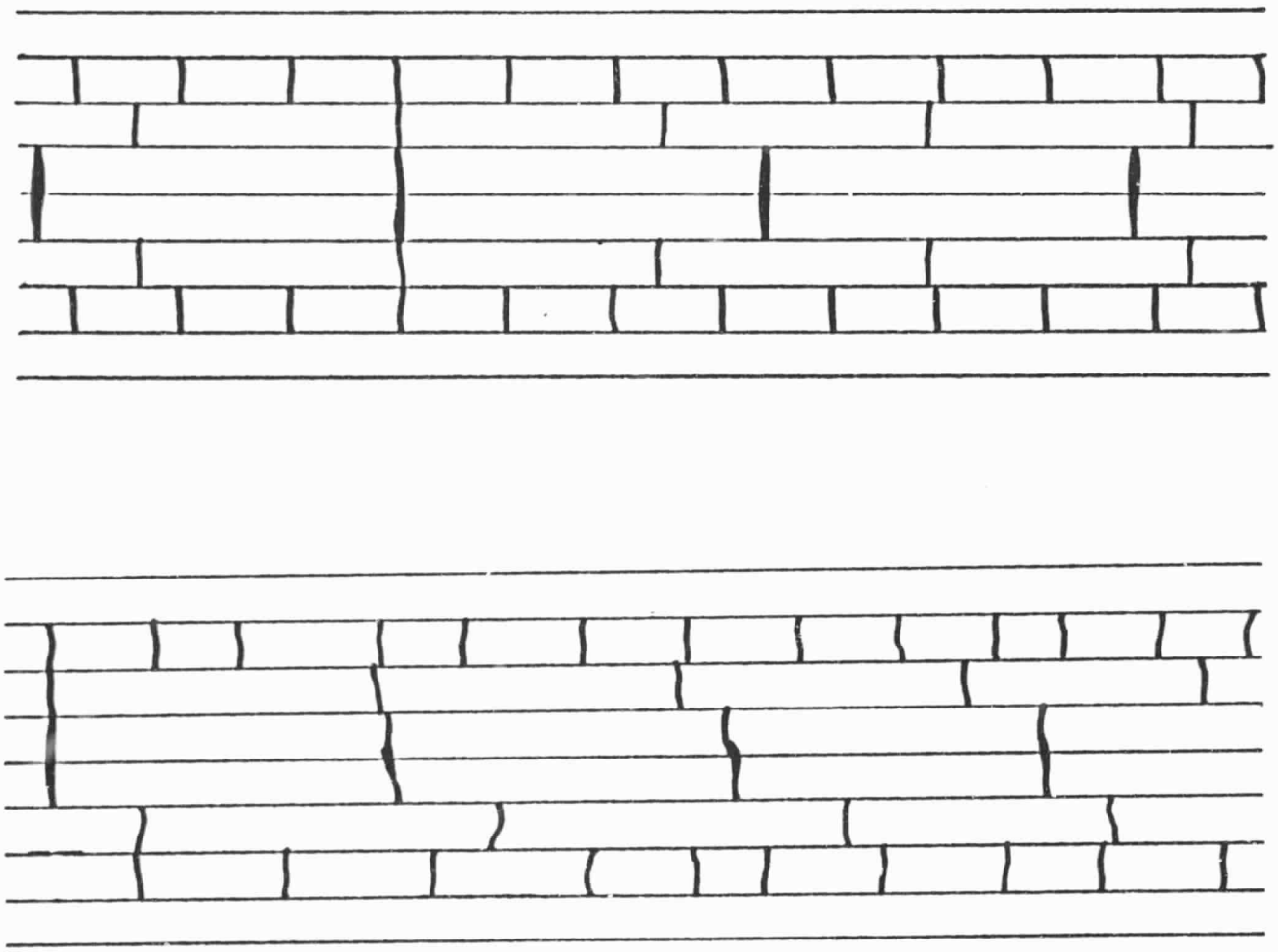

Fig. 24. Observed (top) and Predicted (bottom) Characteristic Damage State for Type II Laminate

damage state for a $[0,90,\pm45]_s$ laminate. (The observed state is on the top and the predicted one is on the bottom.) This characteristic damage state is created at moderate quasi-static loads or by cyclic loading. The plies which form cracks are determined by the magnitude of the load level, but the total number of cracks in the equilibrium characteristic damage state in a given ply is a laminate property, independent of load history or geometry. This characteristic damage state (CDS) controls the state of stress and state of strength in the laminate until the final failure events begin, quite close to fracture. The CDS is a direct result of through-the-thickness constraint stresses which control its formation.

The second basic consequence of through-the-thickness stresses is, as mentioned earlier, the influence of those stresses on notch or flaw growth along laminae boundaries. This effect can also be modelled, but the model must be accurate enough to give fairly reliable three-dimensional (complete) field stress information. Such an analysis was developed in our laboratories under a contracted investigation sponsored by Wright-Patterson Air Force Base (contract no. F33615-77-C-5044). The analysis is a three-dimensional finite difference scheme which can calculate complete stress fields for the cracked lamina problem.

Although the one dimensional analysis discussed earlier is very convenient and instructive, the details of the mechanics involved in crack formation and especially crack growth can not be extracted from such an analysis. The precise nature of the stress field in the neighborhood of a crack in an off-axis ply will determine how that crack grows into the next ply, or along the ply interfaces, or couples with other cracks, or

participates in a laminate fracture event. The mechanics of these important aspects must be investigated by means of a more general and more precise analysis scheme. To investigate the nature of such stress fields in composite laminates with internal cracks transverse to the direction of loading the following model was developed.

It is assumed that the laminate is infinitely wide, and that the cracks extend across the width. Therefore, the stresses are independent of y (Fig. 25). The equilibrium conditions then become:

$$\frac{\partial \sigma_x}{\partial x} + \frac{\partial \tau_{xz}}{\partial z} = 0$$

$$\frac{\partial \tau_{xy}}{\partial x} + \frac{\partial \tau_{yz}}{\partial z} = 0 \qquad (1)$$

$$\frac{\partial \tau_{xz}}{\partial x} + \frac{\partial \sigma_z}{\partial z} = 0 \ .$$

Based on this assumption, and with the aid of the constitutive relations for the material system under consideration, the y dependence of the displacements u, v and w (in the x, y and z directions respectively) can be determined analytically. Accounting for the symmetry conditions, the functional forms of these displacements are found to be:

$$\begin{aligned} u(x,y,z) &= U(x,z) \\ v(x,y,z) &= V(x,z) + Cy \qquad (2) \\ w(x,y,z) &= W(x,z) \end{aligned}$$

Through the use of the strain-displacement relations it can be observed that the displacement field given by equations 2 represent

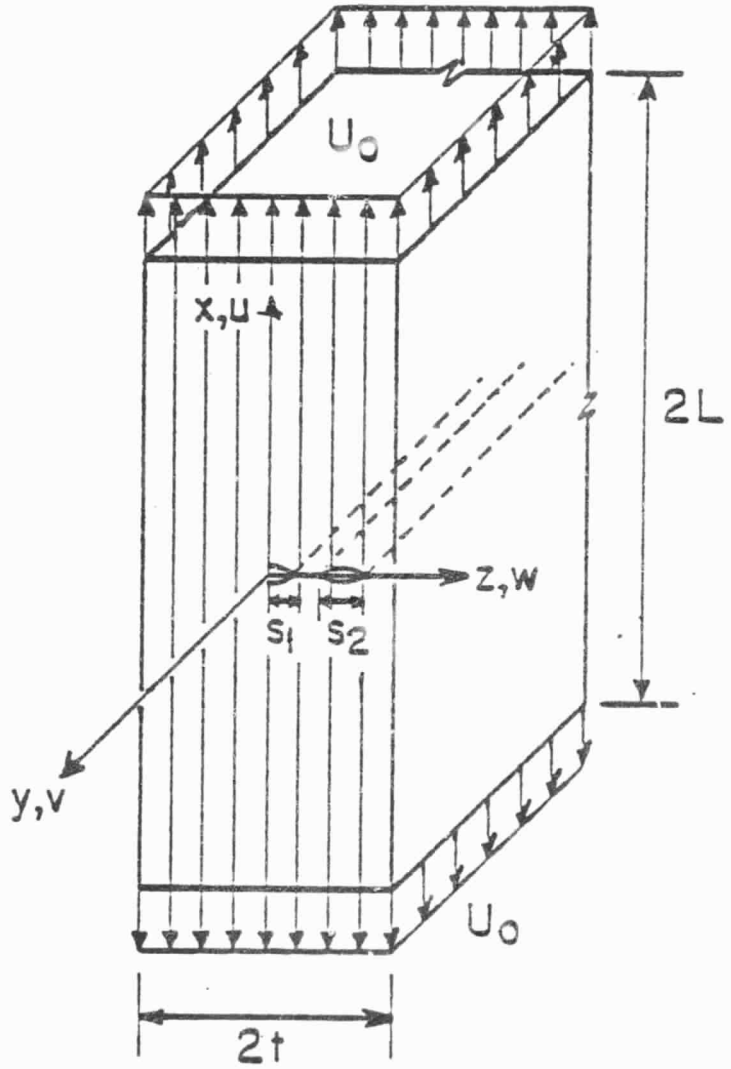

Fig. 25. Schematic diagram of the cracked laminate

the generalized plane strain problem of elasticity. The constant, C, represents the normal strain in the y direction. Due to the symmetric nature of the problem, equations 1 need only be solved within the first quadrant of the x-z plane. A numerical solution to these equations is obtained by expressing the stress components in terms of the displacements, and employing a finite difference discretization scheme. This way, equations 1 are reduced to a set of coupled linear algebraic equations in the unknown nodal values of U, V and W that must be satisfied at all nodal points of the finite difference grid. For improved accuracy near boundaries, equations 1 are satisfied not only at all interior nodes, but also at the boundary nodes. The resulting unknown fictitious nodal values outside the physical domain are evaluated with the aid of boundary conditions discretized by central differences. These are:

$$U(L,z) = U_0$$

$$V(L,z) = W(L,z) = 0 \tag{3}$$

$$\left.\frac{\partial U}{\partial z}\right|_{z=0} = \left.\frac{\partial V}{\partial z}\right|_{z=0} = \left.\frac{\partial^2 W}{\partial z^2}\right|_{z=0} = 0 \tag{4}$$

$$\left.\frac{\partial^2 U}{\partial x^2}\right|_{x=0} = \left.\frac{\partial V}{\partial x}\right|_{x=0} = \left.\frac{\partial W}{\partial x}\right|_{x=0} = 0 \tag{5}$$

$$\sigma_z(x,t) = \tau_{zy}(x,t) = \tau_{zx}(x,t) = 0 \tag{6}$$

When a transverse crack exists in the y-z plane, conditions 6 are replaced by

$$\sigma_x(0,z) = \tau_{xy}(0,z) = \tau_{xz}(0,z) = 0 \tag{7}$$

over that part of the boundary where $z \in (S_1 \text{ or } S_2)$. A complete mathematical treatment of this formulation is given in Reference [7].

Some of the stress distributions in damaged laminates obtained by the use of this analysis are presented in the following section. The applied strain values for all examples discussed here are:

$$\varepsilon_x = 10^{-3} \text{ in/in}$$

and

$$\varepsilon_y = -2 \times 10^{-4} \text{ in/in} .$$

Figure 26 shows the axial normal stress through the laminate thickness for three laminates when the interior plies always consist of a pair of 0° laminae with a center notch. The ordinate of the figure is actually the stress elevation due to the notch for three different constraint layers. Interestingly enough, the lowest modulus (and strength) constraint layer has the highest stress elevation due to a notch. Figures 27 and 28 show a stress that would be completely absent in an unnotched laminate. The through-the-thickness shear stress, τ_{xz}, comes about because the broken lamina tries to "slide out" in a manner similar to our earlier discussion for the in-plane problem. From the standpoint of damage growth this stress contributes to growth between the plies, i.e., a spread of damage above and below the notch or ply crack. The magnitude of the calculated stresses is quite high, high enough to participate in damage growth. The distribution of shear stress for the two laminates is quite similar suggesting that the 0° plies control that distribution.

Figure 29 shows another stress component that is entirely caused

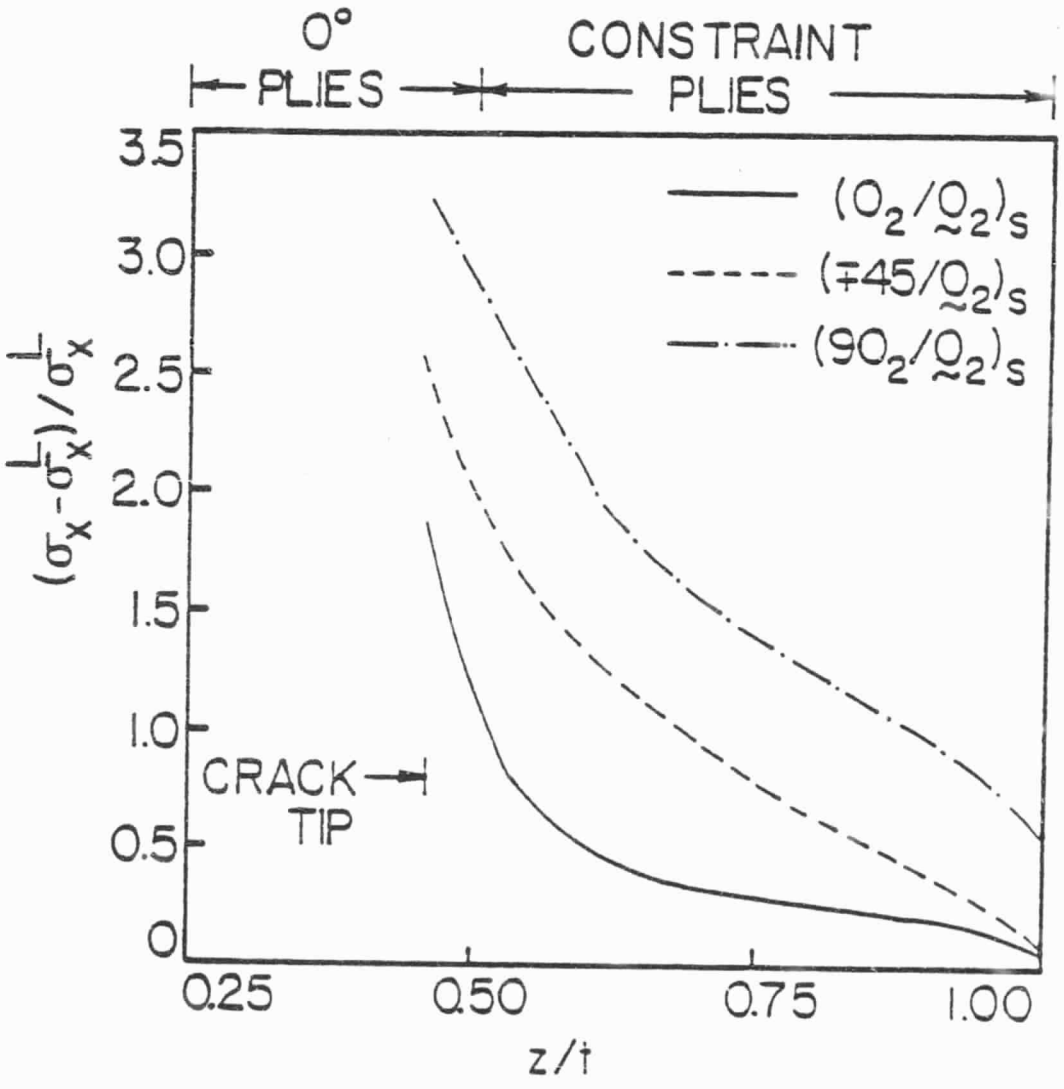

Fig. 26. Normalized stress increase across specimen thickness for a notched 0° ply constrained by three different orientations of constraining plies.

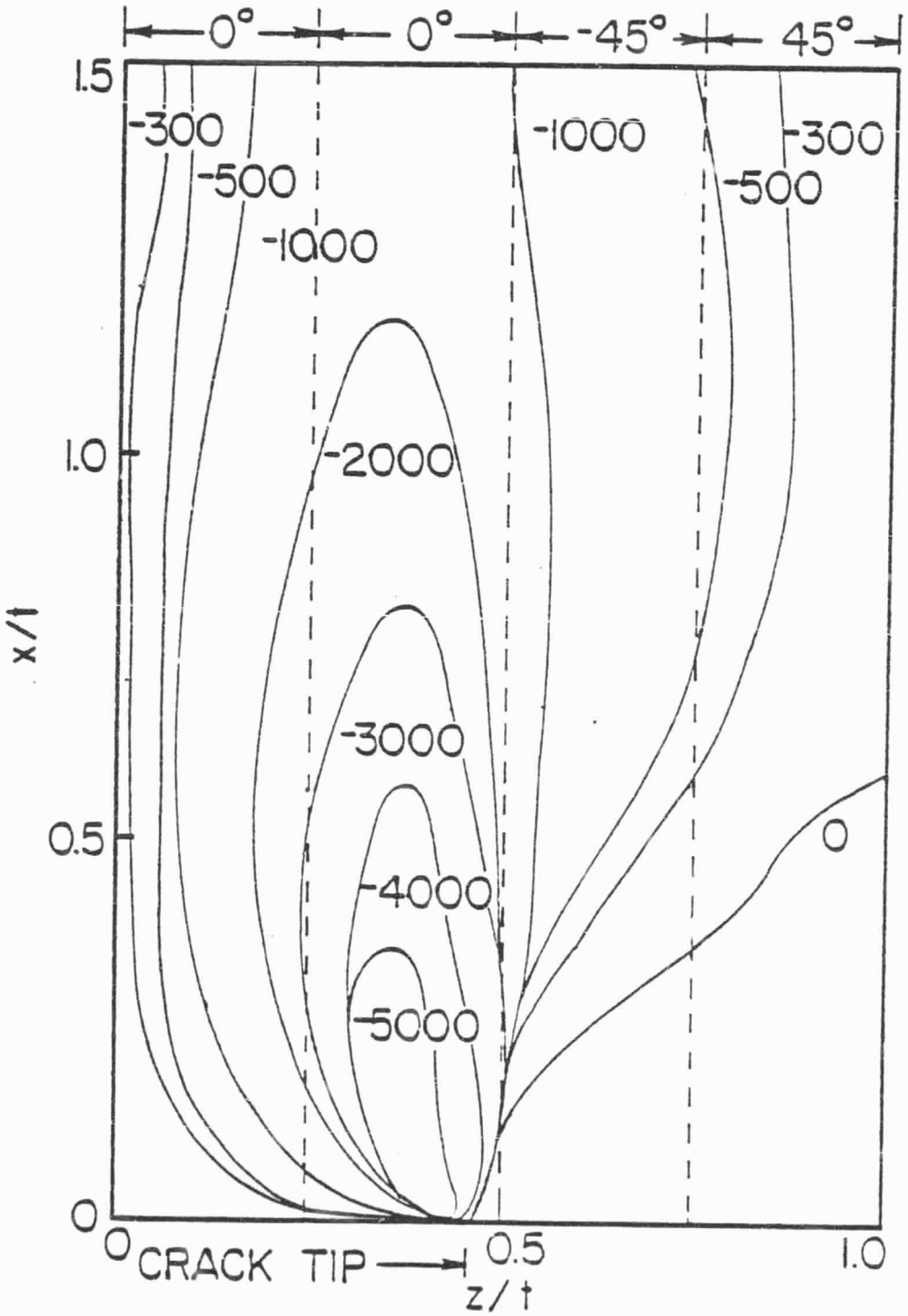

Fig. 27. Contours of τ_{xz} (psi) for a $(\mp 45/0_2)_s$ laminate with 0° ply damage.

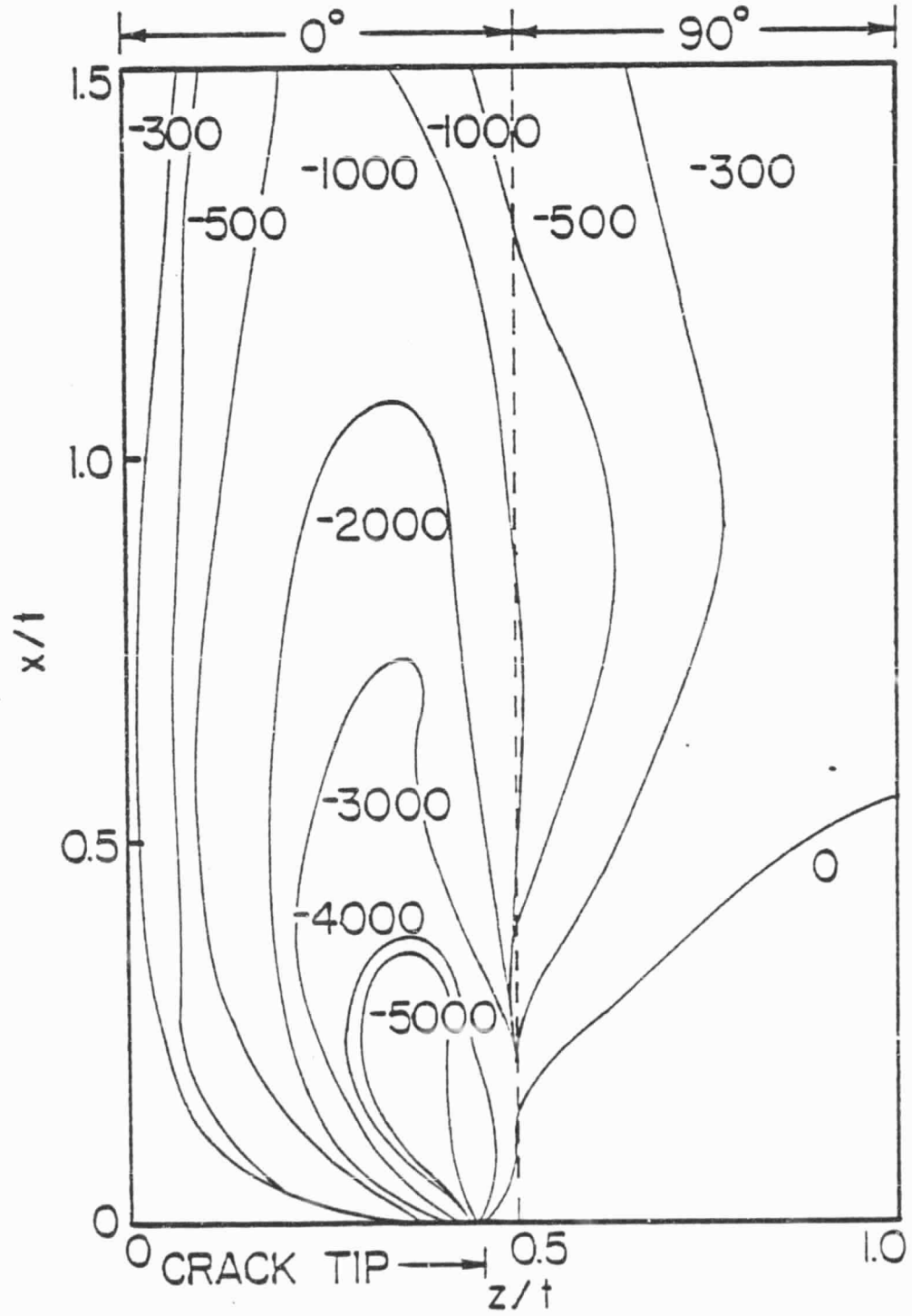

Fig. 28. Contours of τ_{xz} (psi) for a $(90_2/0_2)_s$ laminate with 0° ply damage.

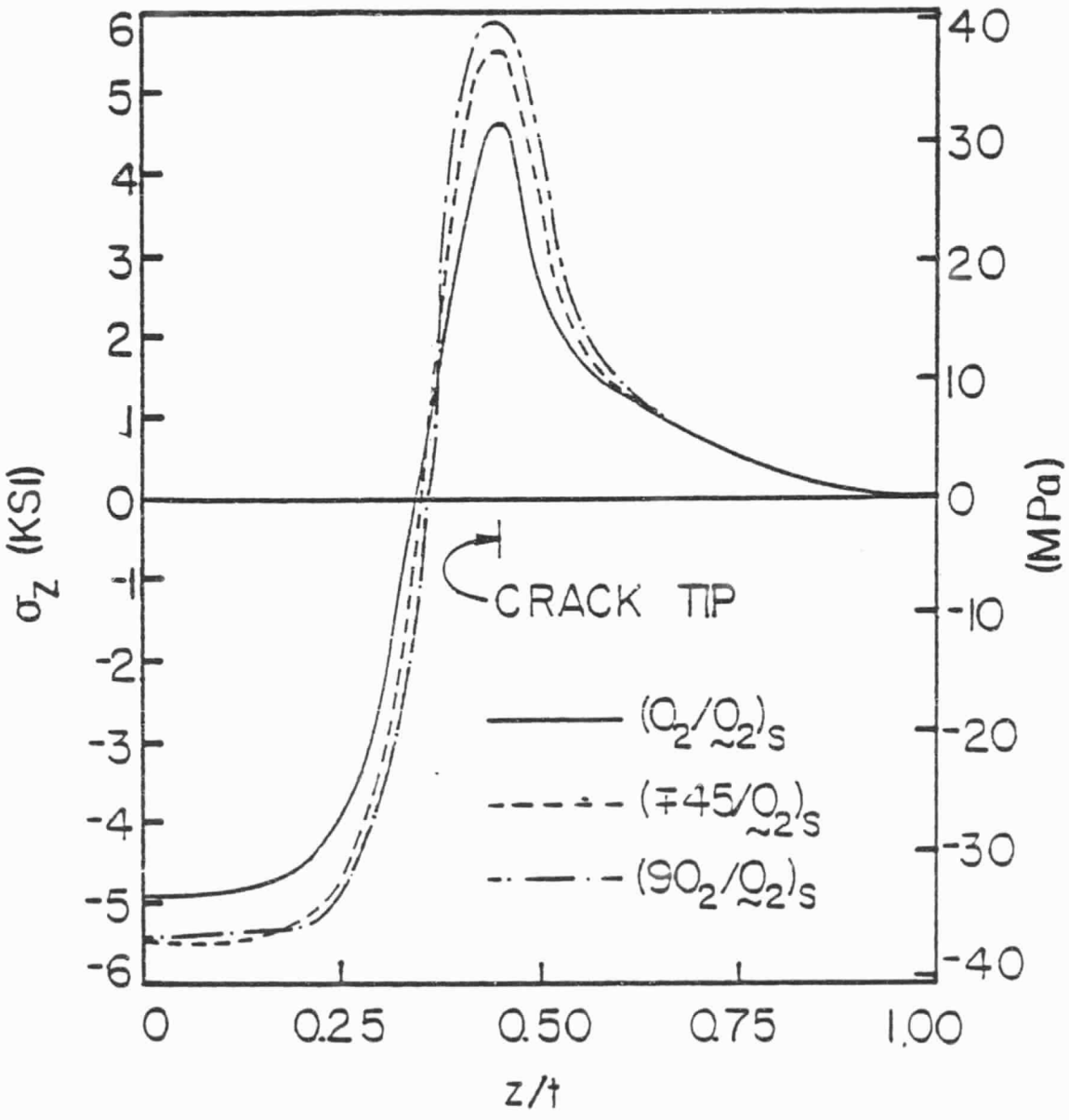

Fig. 29. Constraint effect on the through-the-thickness interlaminar normal stress distribution

by the internal crack or notch. It is a through-the-thickness normal stress, σ_z, which develops at the interface between the broken and unbroken plies. The three constraint situations discussed earlier are shown. Again, the $[90,0]_s$ case shows the greatest σ_z stress. The σ_z component of stress would be expected to produce delamination modes of damage, and the stress levels calculated are significant. As we have shown in the sections on experimental results, the $[90,0]_s$ laminates delaminated extensively in the neighborhood of the notch, and continued to delaminate above and below the longitudinal crack that grew away from the notch tips. Hence, there is ample evidence that the model is helping to anticipate the details of constraint-stress-controlled flaw growth. Such a modelling scheme could also be applied to failure-theory analysis to predict flaw growth through the thickness as well as along ply boundaries.

CONCLUSIONS

A systematic investigation of the effects of constraint on flaw growth and material response has been conducted for several basic situations. The investigation included studies of notched and unnotched laminae, notched and unnotched laminates, several orientations of notch axis with respect to load and principal ply directions, and several orientations of constraining plies. The approach to the study of constraint effects included static tensile and cyclic tension-tension loading, a number of nondestructive investigations to detect and monitor the damage state, sectioning studies, stiffness measurements, and residual strength determinations. The experimental program was complemented by an analysis of the characteristic damage state in unnotched laminates and a stress analysis of laminates with constrained (embedded) flaws.

The response of laminates containing embedded flaws in 90° plies constrained by 0° and ±45° plies was found to be sensitive to defects in the 90° plies. However, the critical defects were not necessarily the intentional flaws put in the specimens during the fabrication process. In a number of cases, the failure of these laminates was due to an inherent unintentional defect and was independent of the intentional defect. Although many cracks will develop in the 90° plies during static and cyclic loading, the collective effect of these cracks on laminate response cannot be ignored. The transverse cracks in 90° plies of quasi-isotropic laminates, for example, develop in a regular and predictable fashion and form the basis of the characteristic damage state which controls subsequent response of the laminates. However, the

spacing of the cracks in all off-axis plies is dependent on the constraint imposed on those plies by adjacent plies.

The response of laminates containing constrained 0° plies was evaluated in terms of the nominal stress in the 0° plies and the strength of notched and unnotched 0° specimens. This proved to be an effective method for comparing the response of laminae under different constraint situations.

The effect of constraint on the response of composite materials can be classified in two categories: (a) in-plane effects and (b) through-the-thickness effects. In-plane constraint is the principal contributor to notched strength and changes in notched strength under quasi-static loading. Damage initiation, which occurs during the first loading cycle at stress levels of practical importance, can be described in terms of in-plane constraint effects. The modes and extent of damage which develop follow from the stress state and distribution of stresses in the constrained plies. The damage modes in the constrained plies are due to the in-plane shear stress and the transverse normal stress components as determined by the orientation of the constraining plies. However, constraint situations which produce greatest static strength do not minimize the extent of damage which develops during static or cyclic loading. Likewise minimum damage situations do not correspond to maximum strength cases.

Growth of damage during cyclic loading is due to through-the-thickness constraint effects. The response of unnotched laminates to static and cyclic loads is controlled by the characteristic damage state which forms independently of the loading history. Damage modes in a

laminate are dependent on the stacking sequence, and the distribution of a particular damage mode in a given ply is sensitive to the constraints imposed on that ply by surrounding plies. Damage in quasi-isotropic laminates with a $[0,\pm45,90]_s$ stacking sequence, for example, consists of transverse cracks in the 45° and 90° plies, longitudinal cracks along the ±45° ply interface, and delaminations between the 90° plies. When the stacking sequence is varied to $[0,90,\pm45]_s$, the in-plane stresses in a particular ply are identical to the in-plane stresses in plies of corresponding orientation in the first laminate. Although transverse and longitudinal cracks still form, the delamination mode of damage is suppressed in the second laminate. Within the 90° plies of each laminate, the distribution of transverse cracks is governed by the orientation of adjacent plies as it determines the distance over which stress is transferred back into the cracked ply.

Out-of-plane stresses produced by constraints are influential on the growth of damage along ply interfaces. This is especially important during cyclic loading. The gradient of interlaminar shear stress τ_{xz} near the flaw is greater in $[90,0]_s$ notched laminates than in $[\pm45,0]_s$ laminates. Also the interlaminar normal stress σ_z near the flaw is greater in the $[90,0]_s$ laminate than in the $[\pm45,0]_s$ laminate. During cyclic loading, the growth of damage (delaminations and cracks parallel to the fibers) is much more extensive when notched 0° plies are constrained by 90° plies than when the same plies are constrained by ±45° plies, even when the nominal stress in the constrained plies is the same. Furthermore, damage in $[90,0]_s$ laminates continues to grow during cyclic loading; but damage in $[\pm45,0]_s$ laminates may arrest or grow at a slower rate. The growth of damage during cyclic loading is also reflected

by the change in stiffness, which was greater for $[90,0]_s$ laminates than for $[\pm 45,0]_s$ laminates under the same nominal cyclic 0° ply stress.

Finally, the mode of damage and the extent of damage in constrained notched and unnotched plies and subsequent changes in material properties is governed by the stress state in those plies, as determined by the constraining plies, and the relationship of the stress state to the strength state. The results of the present program have increased our knowledge and contributed to our understanding of constraint and its effect on composite materials response. However, a complete understanding of all aspects of constraint, especially how it controls the fracture event, has not as yet been achieved. This understanding will only come through the proper coupling of mechanics with materials response in carefully planned and carried out investigations.

REFERENCES

1. Stinchcomb, W. W. and Reifsnider, K. L., "Fatigue Damage Mechanisms in Composite Materials: A Review," ASTM STP 675, 1979.

2. Stinchcomb, W. W., Reifsnider, K. L., Yeung, P., and O'Brien, T. K., "Investigation and Characterization of Constraint Effects on Flaw Growth During Fatigue Loading of Composite Materials," Semi-Annual Status Report, NASA Grant NSG-1364, June 1977.

3. Stinchcomb, W. W., Reifsnider, K. L., Yeung, P., and O'Brien, T. K., "Investigation and Characterization of Constraint Effects on Flaw Growth During Fatigue Loading of Composite Materials," Second Semi-Annual Status Report, NASA Grant NSG-1364, January 1978.

4. Stinchcomb, W. W., Reifsnider, K. L., Yeung, P., "Investigation and Characterization of Constraint Effects on Flaw Growth During Fatigue Loading of Composite Materials," Third Semi-Annual Status Report, NASA Grant NSG-1364, June 1978.

5. Zweben, C., "On the Strength of Notched Composites," J. Mech. Phys. of Solids, Vol. 19, 1971, pp. 103-116.

6. Kulkarni, S. V., McLaughlin, P. V., Jr., and Pipes, R. B., "Fatigue of Notched Fiber Composite Laminates," NASA CR-145039, Materials Sciences Corporation, 1977.

7. Talug, A., "Analysis of Stress Fields in Composite Laminates with Interior Cracks," Dissertation, Dept. of Engineering Science and Mechanics, College of Engineering, VPI & SU, August 1978.